

Cooperative Multi-Bitrate Video Caching and Transcoding in Multicarrier NOMA-Assisted Heterogeneous Virtualized MEC Networks

Sepehr Rezvani, Saeedeh Parsaeefard, *Senior Member, IEEE*, Nader Mokari, *Member, IEEE*, Mohammad R. Javan, *Member, IEEE*, and Halim Yanikomeroglu, *Fellow, IEEE*

Abstract

Cooperative video caching and transcoding in mobile edge computing (MEC) architecture is a new paradigm for future wireless networks, e.g., 5G and 5G beyond, enabling them to utilize scarce and expensive network resources in a more efficient manner. Integration of this technique with other advent technologies, such as network virtualization and multicarrier non-orthogonal multiple access (MC-NOMA), provides more flexible video delivery opportunities for the system, which leads to enhancements both for the network's revenue and for the end-users' service experience. This calls to study related resource allocation frameworks (RAFs) that is the main goal of this paper. Here, we propose a two-phase RAF for a parallel cooperative joint multi-bitrate video caching and transcoding in heterogeneous virtualized MEC networks. In the cache placement phase, we propose novel delivery-aware cache placement strategies (DACPSs) by jointly allocating physical resources and request scheduling based on stochastic video popularity and channel distribution information to exploit flexible delivery opportunities. Then, for the delivery phase, we propose a delivery policy for given caching status, instantaneous requests of users, and channel state information. The optimization problems corresponding to both phases aim

Sepehr Rezvani and Nader Mokari are with the Department of Electrical and Computer Engineering, Tarbiat Modares University, Tehran, Iran.

Saeedeh Parsaeefard is with Communication Technologies & Department, ITRC, Tehran, Iran and University of Toronto (saeideh.fard@utoronto.ca, s.parsaeifard@itrc.ac.ir).

Mohammad R. Javan is with the Department of Electrical and Robotics Engineering, Shahrood University of Technology, Shahrood, Iran.

H. Yanikomeroglu is with the Department of Systems and Computer Engineering, Carleton University, Ottawa, ON K1S 5B6, Canada (E-mail: halim@sce.carleton.ca).

to maximize the total revenue of slices subject to the quality of services contracted between slices and end-users and the system constraints based on their own assumptions. Both problems are non-convex and suffer from high-computational complexities. For each phase, we show how these two problems can be solved efficiently. We also propose a low-complexity RAF in which the complexity of the delivery algorithm is significantly reduced. Extensive numerical assessments demonstrate a performance improvement of up to 30% for our proposed DACPSs over traditional approaches.

Index Terms– Mobile edge computing, cooperative caching, multi-bitrate video transcoding, adaptive bitrate streaming, wireless network virtualization, multicarrier NOMA.

I. INTRODUCTION

A. Background & Motivations

Wireless edge caching has been developed as a candidate solution for next generation wireless networks, e.g., 5G, to address high data rate and/or low latency multimedia services by proactively storing contents at the edge of wireless networks and in so doing offloading scarce and expensive backhaul links [1]–[3]. Among various mobile services, mobile video services and applications are expected to account for a major percentage of the global mobile data traffic in coming years [4], [5]. For this reason, video caching at the network edge has drawn a lot of attention recently [2], [4]–[9].

In practical scenarios, due to the multiple bitrate variants of each unique video file, service providers often need to transcode video files into multiple bitrates [5]–[9]. To this end, adaptive bit rate (ABR) streaming techniques have been developed to enhance the quality of delivered video in radio access networks (RANs) where each video file is adjusted according to users' requests based on their display size and network channel conditions [5]–[7].

Recently, mobile edge computing (MEC) networks have emerged as a promising technology for next generation wireless networks, providing cloud caching and computing capabilities within the RAN [8], [10]–[13]. Thanks to this paradigm, video files could be prefetched and/or transcoded in close proximity to end-users, leading to enormous latency and backhaul traffic reductions in wireless networks. One problem with this, however, is that duplicated video caching and transcoding in multiple resource-constrained MEC servers wastes both storage and processing resources. To tackle this issue, cooperative joint multi-bitrate video caching and transcoding (CVCT) technology is proposed where each MEC server is able to receive the requested video files from neighboring MEC servers via fronthaul links [7]. In this architecture, each MEC server

is deployed side-by-side with each base station (BS) using the generic computing platforms which provides the caching and computation capabilities in heterogeneous networks (HetNets) [7], [8]. By sharing both the storage and processing resources among multiple MEC servers, more video files can be served within the RAN, reducing the backhaul traffic. However, non-simultaneous transferring and transcoding video files wastes more time and physical resources in the CVCT system, which is not beneficial for delay-sensitive services. To cope with this challenge, parallel video transmission and transcoding capability [9], [14] can be deployed. In the parallel CVCT system, video transcoding runs in parallel with video transmission, and all the multi-hop video transmissions (between backhaul, fronthaul, and wireless access links) also run in parallel.

Non-orthogonal multiple access (NOMA) has recently emerged as a key enabling technology to improve the spectral efficiency of 5G wireless networks [15], [16]. Unlike conventional orthogonal multiple access (OMA) techniques, NOMA can significantly improve the system throughput and support the massive connectivity by using successful interference cancellation (SIC) at the receivers and a mixture of multiple messages at the transmitter [15], [16]. The spectral efficiency can be further improved by combining NOMA with multicarrier systems, called multicarrier NOMA (MC-NOMA), which utilizes multicarrier diversity [17]. To reduce the capital expenses (CapEx) and operation expenses (OpEx) of RANs, wireless network virtualization technology is developed where the wireless network infrastructure is abstracted and sliced based on different services [18]–[20]. Exploiting MC-NOMA in virtualized networks can further reduce the wireless bandwidth cost of slices by reusing each subcarrier for multiple users owned by each slice. In this way, the integration of the aforementioned technologies enables the CVCT technology at MEC servers and network infrastructure abstraction for different cost-efficient wireless servicing.

Transcoding a large number of videos at each resource-constrained MEC server simultaneously poses another challenge for delay-sensitive services [5]–[7]. The significant performance gain of the CVCT system can only be achieved when a joint distributed video caching and transcoding strategy is designed [7]. Accordingly, the major question is *which bitrate variant of a video file should be cached or transcoded to another lower bitrate variant?* An efficient design of joint power and subcarrier allocation is required to achieve the benefits of MC-NOMA in the virtualized wireless networks as well as the improved throughput. Additionally, the scheduler should be fast enough to readopt the video delivery policy based on the arrival requests of users and channel state information (CSI), specifically in realistic ultra dense 5G wireless networks with a larger number of videos. To this end, the video delivery policy needs to be lightweight.

Recently, designing efficient cache placement strategies (CPSs) under the consideration of transmission strategies has become more attractive to utilize the physical-layer delivery opportunities in order to have an efficient delivery performance [3]–[5], [21], [22]. In this context, unlike in conventional baseline popular/bitrate video CPSs, we can improve the performance of the proactive video CPSs by utilizing the delivery opportunities, i.e., designing a delivery-aware CPS (DACPS). Despite the huge potential, designing an efficient DACPS needs to address the following challenges: **1) A DACPS should be efficient for the long-term of the next delivery phase.** This algorithm should cover all the delivery moments and also be efficient in the long-term. Therefore, appropriate methodologies have to be devised to handle the variations of CSI and requests of users in different moments of the next delivery phase. In other words, some estimation approaches should be performed in the proactive DACPS design. **2) A DACPS should efficiently utilize the delivery opportunities.** To consider all the transmission and transcoding technologies in the design of an efficient DACPS with a preferable delivery observation, joint optimization of the available physical resources, such as storage, transmission, and processing with user association and request scheduling decisions is required. The output of this optimization is only the video placement.

B. Related Works

Roughly speaking, all research on wireless edge caching can be classified into two categories: 1) delivery performance analysis for different CPSs; 2) designing CPSs in order to have an efficient delivery performance. In the first category, [23] and [24] investigate the benefits of designing joint user association and radio resource allocation for different CPSs. The authors in [23] proposed a joint resource allocation and user association algorithm in orthogonal frequency division multiple access (OFDMA)-based fronthaul capacity constrained cloud-RANs (C-RANs) in order to minimize the network delivery cost. In [24], the authors devised a joint resource allocation and user association algorithm in HetNets with device-to-device (D2D) communications to maximize the user revenues. In the second category, some work has been done to investigate the benefits of considering transmission opportunities in the CPS design for different cache-assisted schemes, such as backhaul-limited networks [2]–[4], [18], [25], cooperative transmission networks [22], [26], cooperative caching networks [27], joint cooperative caching and transmission networks [1], [21], NOMA-assisted networks [15], [16], [28], [29], and network

virtualization [18]–[20], [30]. However, none of these works have utilized the benefits of video transcoding in their systems.

In the context of cloud-based video transcoding, some research efforts investigate the advantages of cloud computing and devise joint processing resource allocation and scheduling policies to reduce the transcoding delays in the delivery phase [9], [31]. In addition, [5]–[7] investigate joint multi-bitrate video caching and transcoding by utilizing the ABR streaming technology in C-RANs. In [6], a transmission-aware joint multi-bitrate video caching and transcoding policy is devised to maximize the number and quality of concurrent video requests in each time slot in a single-cell scenario. In [5], the benefits of joint caching and radio resource allocation policy is investigated for a multi-cell MEC network without any cooperation between MEC servers. Additionally, [7] investigates the design of a transcoding-aware cache replacement strategy in the online delivery phase of a non-parallel CVCT system based on the arrival video requests. Accordingly, designing an efficient proactive DACPS for the CVCT systems is still an open problem. Furthermore, the parallel transmission and transcoding capability is not applied for the CVCT system in [7] which can avoid wasting time and physical resources. Besides, prior works do not utilize the benefits of jointly allocating physical resources for designing an efficient DACPS. In addition, based on our most up-to-date knowledge, the impact of applying MC-NOMA in virtualized wireless networks in terms of bandwidth cost reduction is not yet addressed in the related works. In our research, we address these aforementioned challenges.

C. Our Contributions

In this paper, we consider a parallel CVCT system in a MC-NOMA-assisted heterogeneous virtualized MEC (HV-MEC) network. This network consists of multiple remote radio systems (RRSs) each equipped with a BS and MEC server that enables the CVCT capability in the network edge. For this setup, we propose a virtualization model and a pricing scheme based on the revenues of slices with a specific QoS. In contrast to [7], where the main goal was only to decrease network cost, we aim to maximize the revenue of slices by jointly increasing slice incomes (which is obtained by providing data rates for own users) and decreasing slice costs. In this network, consuming more physical resources provides more data rates for users, which increases slice incomes. However, this consumption causes a network cost increment that degrades slice revenues. Accordingly, this trade-off should be handled carefully.

To address this, we propose a resource allocation framework (RAF) where network operational time is divided into two phases: a cache placement phase (Phase 1); and a delivery phase (Phase 2). To the best of our knowledge, this paper is the first in the literature to propose efficient DACPSs in a parallel CVCT system for a MC-NOMA-assisted HV-MEC network based on available stochastic wireless channel distribution information (CDI) and video popularity distribution (VPD). This novel strategy is designed on the basis of jointly allocating available physical resources as storage, processing, and transmission (transmit power of RRSs, subcarriers, and backhaul and fronthaul capacities) with user association and request scheduling.

Since the benefits of each component of the CVCT system are not well evaluated numerically in the literature, via simulation results, we investigate the performance gain of each technology in the CVCT system compared to a scenario where no caching or transcoding capabilities are considered for RRSs. Some of these performance gain results are summarized in the following:

- Non-cooperative caching with no transcoding: 459.8%
- Non-cooperative caching and transcoding: 982.9%
- Cooperative caching with no transcoding: 1076.8%
- Cooperative caching and transcoding: 1740.2%

This work can be considered a benchmark for future HV-MEC networks. Extensive numerical results show that MC-NOMA outperforms the systems revenue nearly 21.91% compared to OMA. Moreover, we show that our proposed DACPSs have up to 30% performance gain in terms of the total delivery revenue of slices compared to the conventional baseline video popularity/bitrate strategies.

This paper also provides a novel solution to reduce the computational complexity of our delivery algorithm with on-demand and real-time cloud services. We show that our proposed low-complexity RAF (LC-RAF) can be efficiently utilized for dense environments where there are higher levels of path loss.

D. Paper Organization

The rest of this paper is organized as follows. Section II presents the network architecture and formulates the cache placement and delivery optimization problems. Section III contains the solution of the problems and the proposed LC-RAF. The numerical results are presented in Section IV. Our concluding remarks are provided in Section V. The abbreviations used in the paper are summarized in Table I.

TABLE I: Abbreviations.

Abbreviation	Definition	Abbreviation	Definition
ABR	Adaptive bit rate	IPM	Interior-point method
BS	Base station	LC-RAF	Low-complexity RAF
CCNT	Cooperative caching with no transcoding	LD	Low-diversity
CDI	Channel distribution information	LP-RRS	Low-power RRS
CPS	Cache placement strategy	MBS	Macro BS
C-RAN	Cloud-RAN	MC-NOMA	Multicarrier NOMA
CSI	Channel state information	MEC	Mobile edge computing
CVCT	Cooperative video caching and transcoding	MINLP	Mixed-integer nonlinear programming
D.C.	Difference-of-two-concave-functions	MPV	Most popular video
DACPS	Delivery-aware CPS	NC	No caching
DCP	Disciplined convex programming	NoCoop	Non-cooperative
FBS	Femto BS	OMA	Orthogonal multiple access
HBV	High-bitrate video	PSD	Power spectral density
HD	High-diversity	RAF	Resource allocation framework
HP-RRS	High-power RRS	RAN	Radio access network
HV-MEC	Heterogeneous virtualized MEC	RRS	Remote radio system
IDCP	Integer disciplined convex programming	SCA	Successive convex approximation
INLP	Integer nonlinear programming	SIC	Successful interference cancellation
InP	Infrastructure provider	VPD	Video popularity distribution

II. SYSTEM MODEL AND PROBLEM FORMULATION

A. Network Architecture and System Settings

Consider a multiuser HV-MEC network consisting of multiple RRSs, each equipped with one type of access node, e.g., macro BS (MBS) or femto BS (FBS), and a MEC server that enables video caching and transcoding capabilities at the RRS [7], [8]. The set of users and RRSs are denoted by $\mathcal{U} = \{1, \dots, U\}$ and $\mathcal{B} = \{1, \dots, B\}$, respectively. All RRSs are connected by a limited wired fronthaul mesh network, which provides cooperative communication between RRSs [7]. An origin cloud server denoted by 0 is connected to each RRS through a limited wired backhaul link. Here, we assume that a hypervisor enables the virtualization of the network where the physical infrastructure provider (InP) is abstracted into a set of $\mathcal{M} = \{1, \dots, M\}$ virtual networks, i.e., slices, such that slice m owns a subset of users in \mathcal{U} , i.e., \mathcal{U}_m , and is responsible for providing a specific QoS for its own users [18], [20]. We assume that each user

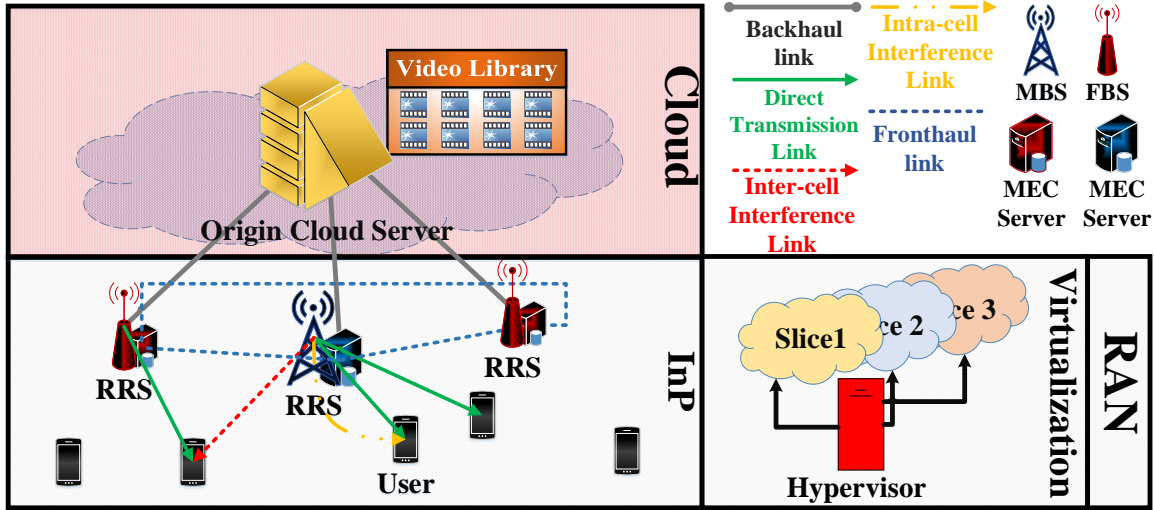


Fig. 1: An example of the multiuser HV-MEC architecture consisting of 3 RRSs, 3 slices, and one InP.

is subscribed to only one slice. Fig. 1 shows an illustration of this network.

Assume that there exist V unique transcodable videos, each having L bitrate variants¹ in the origin cloud server with unlimited storage capacity [5], [7], [22]. The video library is denoted by $\mathcal{V} = \left\{ v_l | v \in \{1, \dots, V\}, l \in \{1, \dots, L\} \right\}$, where v_l belongs to the v^{th} video type with the l^{th} bitrate variant with the size of s_{v_l} . Consider that video v_h can be transcoded to v_l , if $l < h$ [6]–[8]. Note that $s_{v_l} \leq s_{v_h}$, if $l \leq h$ [7].

This network operates in two phases: Phase 1, where the scheduled video files are proactively stored in the cache of RRSs during off-peak times [6], [7]; and Phase 2, where the requested videos are sent to the end-users according to the adopted delivery policy [7], [9], [14], [31]. In Phase 1, we aim to design an efficient DACPS based on the available VPD and CDI. Phase 2, which is followed by Phase 1, is divided into multiple finite time slots where in each time slot, we propose a delivery policy based on the arrival requests of users, CSI, and the caching status. The proposed RAF is illustrated in Fig. 2. To design a DACPS in Phase 1 utilizing the delivery opportunities in the system, we first need to describe the delivery model of the system in Phase 2. Then, we investigate the idea of developing DACPSs in Phase 1.

¹The lowest bitrate of each video type is denoted by 1 and the highest is denoted by L .

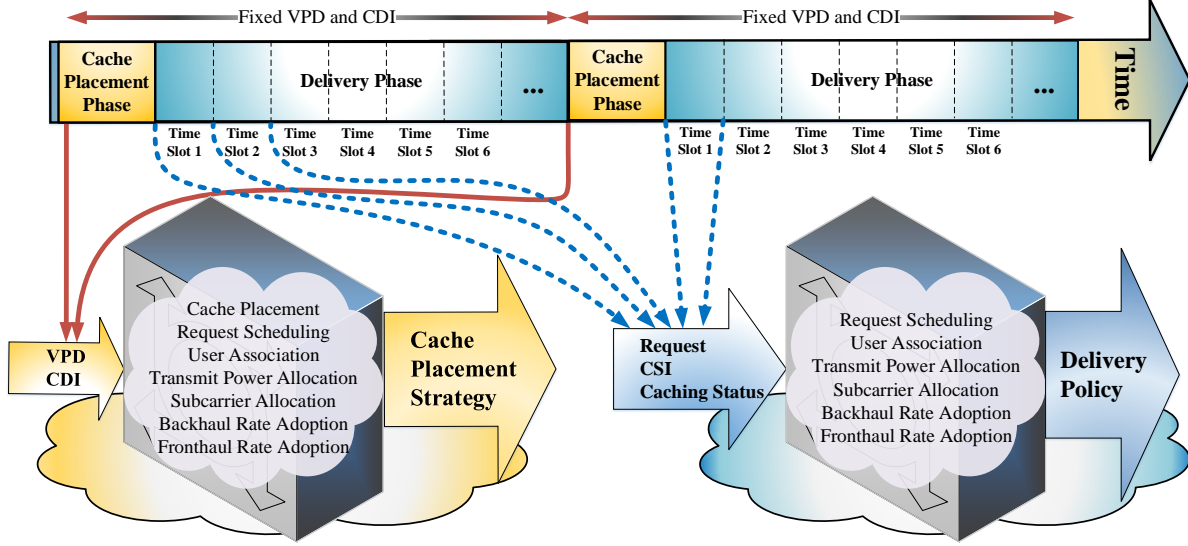


Fig. 2: The proposed two-phase RAF for a parallel CVCT system in HV-MECs.

B. Phase 2

In this phase, we assume a time-slotted system where at the beginning of each time slot, each user requests one video file. Similar to related works [3]–[6], [18], [19], [30], [32]–[34], the CSI and requests of users remain fixed through a time slot and are completely independent from other time slots². All requests of users at each time slot should also be served within the time slot [3], [18], [33]. Hence, the adopted delivery policy for each time slot is completely independent from other time slots. Therefore, we focus on only one time slot in Phase 2. The request of user u for video v_l is indicated by a binary variable $\delta_u^{v_l} \in \{0, 1\}$ such that if user u requests video v_l , $\delta_u^{v_l} = 1$ and otherwise, $\delta_u^{v_l} = 0$. Thus, we have $\sum_{v_l \in \mathcal{V}} \delta_u^{v_l} = 1, \forall u \in \mathcal{U}$. The binary parameter $\theta_{b,u} \in \{0, 1\}$ determines the user association indicator where if user u is associated with RRS b , $\theta_{b,u} = 1$ and otherwise, $\theta_{b,u} = 0$. In this system, we assume that each

²Similar to previous works, the main motivation for considering this model is to simplify the video transmission model. Actually, dynamic video requesting and changes of CSI during each data transmission time cause a more complex delivery model, which is not yet investigated in the joint radio resource allocation and content placement context [3]. Assuming a dynamic video requesting with changes of CSI during a time slot can be considered as a future work.

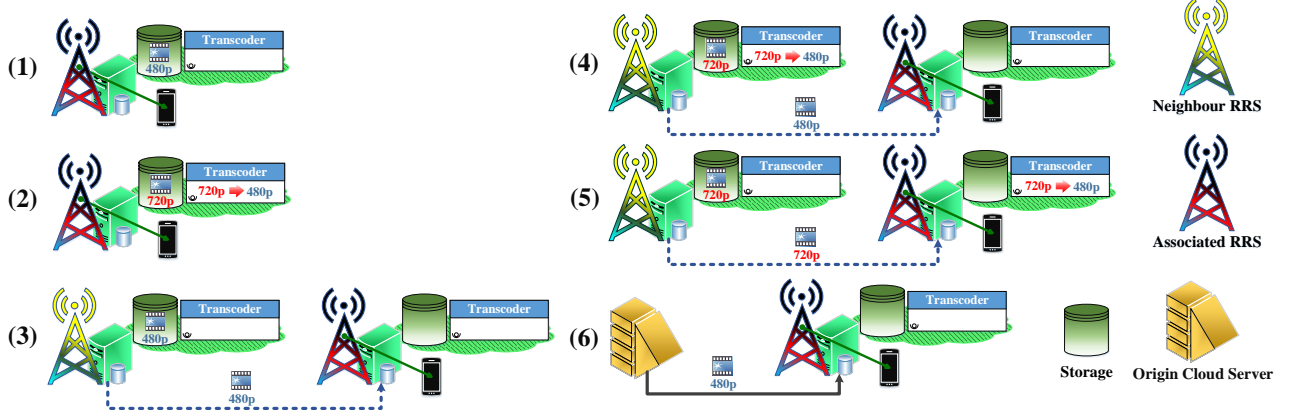


Fig. 3: The possible events of serving a request of a user in the CVCT system. We assume that there are two bitrate variants of a video file at 480p and 720p where the user requests the 480p bitrate variant.

user can be connected to at most one RRS, which is represented by [3], [6], [7], [18], [30]³

$$\sum_{b \in \mathcal{B}} \theta_{b,u} \leq 1, \quad \forall u \in \mathcal{U}. \quad (1)$$

The requests of users associated with RRS b for video v_l can be served by one of the following binary events denoted by [7]:

- 1) $x_b^{v_l} = 1$ represents that video v_l can be sent directly from cache of RRS b .
- 2) $y_b^{v_h, v_l} = 1$ indicates that video v_l is directly served by RRS b after being transcoded from a higher bitrate variant h at RRS b .
- 3) $z_{b',b}^{v_l} = 1$ denotes that video v_l is provided from cache of RRS $b' \neq b$ via fronthaul link.
- 4) $t_{b',b}^{v_h, v_l} = 1$ represents that video v_l is served by transcoding from $v_h, h > l$ at RRS $b' \neq b$ and then, sending to RRS b via fronthaul link.
- 5) $w_{b',b}^{v_h, v_l} = 1$ indicates that video v_l is obtained by sending video $v_h, h > l$ from RRS b' to RRS b via fronthaul link and then, transcoding v_h to v_l at RRS b .
- 6) $o_b^{v_l} = 1$ represents that the requests of users of RRS b for video v_l are served from the origin cloud server via backhaul link b .

Fig. 3 shows all possible events that happen to serve requests for each video file at each RRS. To avoid duplicated video provisioning at each RRS, we assume that all the requests for each

³This parallel CVCT system can also be extended to a coordinated multi-point-enabled one in which each user is able to access to more than one transmitter. Despite the significant potential, the coordinated multi-point system increases the complexity of the delivery model. Therefore, we consider this scheme as a future work.

video file v_l from users associated with RRS b can be served by only one type of events [7], i.e.,

$$x_b^{v_l} + \sum_{\substack{v_h \in \mathcal{V} \\ h > l}} y_b^{v_h, v_l} + \sum_{\substack{b' \in \mathcal{B} \\ b' \neq b}} z_{b', b}^{v_l} + \sum_{\substack{b' \in \mathcal{B} \\ b' \neq b}} \sum_{\substack{v_h \in \mathcal{V} \\ h > l}} \left(t_{b', b}^{v_h, v_l} + w_{b', b}^{v_h, v_l} \right) + o_b^{v_l} = \min \left\{ \sum_{u=1}^U \delta_u^{v_l} \theta_{b, u}, 1 \right\}, \forall b \in \mathcal{B}, v_l \in \mathcal{V}. \quad (2)$$

In practical terms, the video transcoding can only be performed for higher bitrate variants of a transcodable video file to lower bitrate variants. Accordingly, we have $y_b^{v_h, v_l}, t_{b', b}^{v_h, v_l}, w_{b', b}^{v_h, v_l} = 0, \forall h \leq l$ [7], [9]. Note that each event can be chosen if the required video exists in the target storage [6], [7], [9]. Let $\rho_b^{v_l}$ be the binary cache placement indicator where $\rho_b^{v_l} = 1$ if video v_l is cached by RRS b , and $\rho_b^{v_l} = 0$, otherwise. Therefore, we have

$$x_b^{v_l} \leq \rho_b^{v_l}, \quad y_b^{v_h, v_l} \leq \rho_b^{v_h}, \quad z_{b', b}^{v_l} \leq \rho_{b'}^{v_l}, \quad t_{b', b}^{v_h, v_l} \leq \rho_{b'}^{v_h}, \quad w_{b', b}^{v_h, v_l} \leq \rho_{b'}^{v_h}. \quad (3)$$

In this parallel CVCT system, the MC-NOMA technology is deployed at each RRS such that the total frequency bandwidth W is divided into a set of $\mathcal{N} = \{1, 2, \dots, N\}$ orthogonal subcarriers where the frequency band of each subcarrier is W_s . In this scheme, we assume that users aim to download the video files; online video servicing based on the playback rate of videos in the HV-MEC networks is considered for future work. To this end, MC-NOMA allows each orthogonal subcarrier n to be shared among multiple users in each RRS via applying a superposition coding at the transmitter side⁴ and a SIC at the receiver side [17], [35], [36]. The binary subcarrier assignment indicator is also indicated by $\tau_{b, u}^n$, where if subcarrier n is assigned to the channel from RRS b to user $u \in \mathcal{U}$, $\tau_{b, u}^n = 1$ and otherwise, $\tau_{b, u}^n = 0$. Note that each user can take subcarriers from RRS b if the user is associated with that RRS. Therefore, we should have [3], [5], [18]

$$\tau_{b, u}^n \leq \theta_{b, u}, \forall b \in \mathcal{B}, n \in \mathcal{N}, u \in \mathcal{U}. \quad (4)$$

We denote by $p_{b, u}^n$ the transmit power of RRS b to user $u \in \mathcal{U}$ on subcarrier n , and, $h_{b, u}^n$ the instantaneous channel power gain between RRS b and user $u \in \mathcal{U}$ on subcarrier n . After performing SIC, the instantaneous signal-to-interference-plus-noise ratio (SINR) at user $u \in \mathcal{U}$ associated with RRS b on subcarrier n is [17], [35]

$$\gamma_{b, u}^n = \frac{p_{b, u}^n h_{b, u}^n}{I_{b, u}^{\text{Intra}, n} + I_{b, u}^{\text{Inter}, n} + \sigma_{b, u}^n}, \quad (5)$$

⁴During the data transmission time of this parallel system, the transmitter is always able to superpose the received bits of multiple video files.

where $I_{b,u}^{\text{Intra},n} = \sum_{\substack{u' \in \mathcal{U}, u' \neq u \\ h_{b,u'}^n > h_{b,u}^n}} p_{b,u'}^n h_{b,u}^n$ represents the induced intra-cell interference on user $u \in \mathcal{U}$ over subcarrier n , $I_{b,u}^{\text{Inter},n} = \sum_{\substack{b' \in \mathcal{B} \\ b' \neq b}} \sum_{\substack{u' \in \mathcal{U} \\ u' \neq u}} p_{b',u'}^n h_{b',u}^n$ is the received inter-cell interference at user $u \in \mathcal{U}$ over subcarrier n , and $\sigma_{b,u}^n = W_s N_0$ is the additive white Gaussian noise (AWGN) power, in which N_0 is the noise power spectral density (PSD). Therefore, the instantaneous data rate at user $u \in \mathcal{U}$ from RRS b on subcarrier n is $r_{b,u}^n = \tau_{b,u}^n W_s \log_2(1 + \gamma_{b,u}^n)$. To apply the SIC technique for MC-NOMA, the following constraint should be satisfied [17]:

$$\tau_{b,u}^n \frac{p_{b,u'}^n h_{b,u}^n}{\sum_{\substack{v \in \mathcal{U}, v \neq u' \\ h_{b,v}^n > h_{b,u'}^n}} p_{b,v}^n h_{b,u}^n + I_{b,u}^{\text{Inter},n} + \sigma_{b,u}^n} > \tau_{b,u'}^n \gamma_{b,u'}^n, \forall b \in \mathcal{B}, u, u' \in \mathcal{U}, n \in \mathcal{N}, \tau_{b,u}^n, \tau_{b,u'}^n > 0, h_{b,u}^n > h_{b,u'}^n. \quad (6)$$

Accordingly, the instantaneous data rate at user $u \in \mathcal{U}$ assigned to RRS b is $r_{b,u}^{\text{Ac}} = \sum_{n=1}^N r_{b,u}^n$. Under the assumption that each RRS b has a maximum transmit power P_b^{max} , we have

$$\sum_{u \in \mathcal{U}} \sum_{n=1}^N \tau_{b,u}^n p_{b,u}^n \leq P_b^{\text{max}}, \forall b \in \mathcal{B}. \quad (7)$$

Consequently, the instantaneous latency of user u to receive video v_l from RRS b can be calculated as $D_{b,u}^{\text{Ac},v_l} = \frac{s_{v_l}}{r_{b,u}^{\text{Ac}}}$.

Transcoding video v_h to $v_l, \forall l < h$, is performed via the ABR streaming technique where the transcoding operation is mapped to a η^{v_h, v_l} -bits computation-intensive task [7], [8]. Let $N_{\text{Cycle}}^{v_h, v_l}$ be the number of central processing unit (CPU) cycles required to compute 1 bit of the computation-intensive task of transcoding video⁵ v_h to v_l [10], [11]. Each RRS performs all scheduled computation tasks in parallel by efficiently allocating its computation resources [12], [13]. The number of CPU cycles per second allocated to RRS b for transcoding video v_h to v_l is also indicated by $\phi_b^{v_h, v_l} \in \{0, 1, 2, \dots\}$ [9], [10], [31]. Let χ_b^{max} be the maximum processing capacity of RRS b . Therefore, the per-RRS maximum processing capacity constraint can be expressed as

$$\sum_{\substack{v_h \in \mathcal{V} \\ h > l}} \sum_{v_l \in \mathcal{V}} \left(y_b^{v_h, v_l} + \sum_{b' \in \mathcal{B}/\{b\}} t_{b,b'}^{v_h, v_l} + \sum_{b' \in \mathcal{B}/\{b\}} w_{b',b}^{v_h, v_l} \right) \phi_b^{v_h, v_l} \leq \chi_b^{\text{max}}, \forall b \in \mathcal{B}. \quad (8)$$

The speed of the transcoding process is obtained by the video transrating, i.e., transcoding bit rate, which is the number of bits transcoded by the processor per second [14]. Therefore, the delay of transcoding video v_h to v_l at RRS b can be obtained by $D_b^{\text{TC}, v_h, v_l} = \frac{\eta^{v_h, v_l} N_{\text{Cycle}}^{v_h, v_l}}{\phi_b^{v_h, v_l}}$ [11]–[13].

⁵ $N_{\text{Cycle}}^{v_h, v_l}$ is referred to the workload of the task of transcoding video v_h to v_l in the ABR technique.

For this setup, we consider $R_{0,b}^{\max}$ and $R_{b',b}^{\max}$ as the maximum capacity of backhaul link b , and fronthaul link from RRS b' to RRS b , respectively [32]. We also denote $r_{0,b}^{v_l}$ and $r_{b',b}^{v_l}$ the adopted data rate for RRS b to receive video v_l from the origin cloud server and from the neighboring RRS b' , respectively. Hence, the following maximum channel capacity constraints should be satisfied:

$$\sum_{v_l \in \mathcal{V}} o_b^{v_l} r_{0,b}^{v_l} \leq R_{0,b}^{\max}, \forall b \in \mathcal{B}, \quad (9)$$

and

$$\sum_{v_l \in \mathcal{V}} \left(z_{b',b}^{v_l} + \sum_{\substack{v_h \in \mathcal{V} \\ h > l}} t_{b',b}^{v_h, v_l} \right) r_{b',b}^{v_l} + \sum_{v_l \in \mathcal{V}} \sum_{\substack{v_h \in \mathcal{V} \\ h > l}} w_{b',b}^{v_h, v_l} r_{b',b}^{v_h} \leq R_{b',b}^{\max}, \forall b, b' \in \mathcal{B}, b' \neq b. \quad (10)$$

Accordingly, the delays of receiving video v_l from the origin cloud server and RRS b' at RRS b are represented as $D_{0,b}^{\text{BH}, v_l} = \frac{s_{v_l}}{r_{0,b}^{v_l}}$ and $D_{b',b}^{\text{FH}, v_l} = \frac{s_{v_l}}{r_{b',b}^{v_l}}$, respectively.

From the isolation perspective in slicing context, to guarantee the QoS at users owned by each slice m , i.e., \mathcal{U}_m , we apply a minimum data rate constraint as

$$\sum_{b \in \mathcal{B}} r_{b,u}^{\text{Ac}} \geq R_m^{\min}, \forall m \in \mathcal{M}, u \in \mathcal{U}_m, \quad (11)$$

where R_m^{\min} represents the minimum required access data rate of users in \mathcal{U}_m [30]. Satisfying (11) for a non-zero variable R_m^{\min} needs allocating at least one subcarrier to each user in \mathcal{U}_m . According to (4), this condition can only be applied if each user be associated with at least one RRS. Therefore, for each non-zero variable R_m^{\min} , all users in \mathcal{U}_m should be associated with at least one RRS. Accordingly, based on constraints (1), (4), and (11), if $R_m^{\min} > 0$, the inequality in (1) turns into an equality for all users in \mathcal{U}_m . It is noteworthy that $R_m^{\min} = 0$ means slice m does not guarantee any QoS for its own users. In this regard, this slice provides a best-effort service in which the requests of its own users are not guaranteed to be served.

The video transcoding process runs in parallel with the video transmission, where the delay of each transcoding in the system is measured by transcoding the first several segments of a video file [9], [14]. This is negligible compared to the corresponding wireless transmission delay. To efficiently allocate physical resources in this parallel system, some transmission/transcoding delay constraints should be held for each multi-hop scheduling event. For instance, in Event 2, the delay of transcoding video v_h to v_l at RRS b should not be greater than the access latency of user u to receive video v_l from RRS b [6], [14], i.e.,

$$y_b^{v_h, v_l} D_b^{\text{TC}, v_h, v_l} \leq \delta_u^{v_l} D_{b,u}^{\text{Ac}, v_l}. \quad (12)$$

For Event 3, the delay of fronthaul transmission should not be greater than the access delay [30], [32], [33]. Therefore, we have

$$z_{b',b}^{v_l} D_{b',b}^{\text{FH},v_l} \leq \delta_u^{v_l} D_{b,u}^{\text{Ac},v_l}. \quad (13)$$

For Event 4, the delay of transcoding and fronthaul transmission should not be greater than the fronthaul and access delays, respectively. These practical constraints can be represented as

$$t_{b',b}^{v_h,v_l} D_{b'}^{\text{TC},v_h,v_l} \leq t_{b',b}^{v_h,v_l} D_{b',b}^{\text{FH},v_l}, \quad (14)$$

$$t_{b',b}^{v_h,v_l} D_{b',b}^{\text{FH},v_l} \leq \delta_u^{v_l} D_{b,u}^{\text{Ac},v_l}. \quad (15)$$

For Event 5, fronthaul and transcoding delays should not be greater than the transcoding and access delays, respectively. Hence, we have

$$w_{b',b}^{v_h,v_l} D_{b',b}^{\text{FH},v_h} \leq w_{b',b}^{v_h,v_l} D_b^{\text{TC},v_h,v_l}, \quad (16)$$

$$w_{b',b}^{v_h,v_l} D_b^{\text{TC},v_h,v_l} \leq \delta_u^{v_l} D_{b,u}^{\text{Ac},v_l}. \quad (17)$$

Finally, for Event 6, the backhaul delay should be equal or less than the access delay for each video transmission. Accordingly, we have

$$o_b^{v_l} D_{0,b}^{\text{BH},v_l} \leq \delta_u^{v_l} D_{b,u}^{\text{Ac},v_l}. \quad (18)$$

If all conditions in (12)-(18) hold, the total latency of each user comes from its access delay (wireless transmission delay) [14], [22], [30]. This parallel system prevents the extra fronthaul/backhaul transmission and video transcoding delays in the network.

Since slices lease the physical resources of InP, we intend to propose a new pricing model to represent this structure. For the access transmission resources, the unit price of transmit power and spectrum of RRS b are indicated by α_b^{Pow} per Watt and α_b^{Sub} per Hz, respectively [19], [30]. Moreover, the unit price of backhaul and fronthaul rates are defined as α^{BH} and α^{FH} per bps [30]. For the storage resources, each slice pays μ_b^{Cache} per bit to utilize the memory of RRS b [19]. The price of the processing resources usage at RRS b is also defined as μ_b^{Proc} per CPU cycle. On the other hand, each slice m gets rewards from its own users due to providing their access data rates [18], [19], [30]. We define ψ_m as the reward of slice m from each user $u \in \mathcal{U}_m$ per unit of received data rate (bit/s). Let us consider that ψ_m is an increasing function of R_m^{min} , i.e., for $m \neq m' \in \mathcal{M}$, for $R_m^{\text{min}} \geq R_{m'}^{\text{min}}$, we have $\psi_m \geq \psi_{m'}$. In this scheme, we aim to maximize

the revenue of slices, which can be defined as the reward minus cost of each slice. The reward of each slice m is $\sum_{b \in \mathcal{B}} r_{b,u}^{\text{Ac}} \psi_m$. To define the cost of each slice, we first formulate the cost of provisioning video v_l to RRS b caused by one of the scheduling events as

$$\begin{aligned} \mathbb{S}_b^{\text{Cost,RRS},v_l} &= x_b^{v_l} (s_{v_l} \mu_b^{\text{Cache}}) + \sum_{\substack{v_h \in \mathcal{V} \\ h > l}} y_b^{v_h, v_l} (s_{v_h} \mu_b^{\text{Cache}} + \phi_b^{v_h, v_l} \mu_b^{\text{Proc}}) + \sum_{\substack{b' \in \mathcal{B} \\ b' \neq b}} z_{b', b}^{v_l} (s_{v_l} \mu_{b'}^{\text{Cache}} + r_{b', b}^{v_l} \alpha^{\text{FH}}) + \\ &\sum_{\substack{b' \in \mathcal{B} \\ b' \neq b}} \sum_{\substack{v_h \in \mathcal{V} \\ h > l}} t_{b', b}^{v_h, v_l} (s_{v_h} \mu_{b'}^{\text{Cache}} + \phi_{b'}^{v_h, v_l} \mu_{b'}^{\text{Proc}} + r_{b', b}^{v_l} \alpha^{\text{FH}}) + \sum_{\substack{b' \in \mathcal{B} \\ b' \neq b}} \sum_{\substack{v_h \in \mathcal{V} \\ h > l}} w_{b', b}^{v_h, v_l} (s_{v_h} \mu_{b'}^{\text{Cache}} + r_{b', b}^{v_h} \alpha^{\text{FH}} + \\ &\phi_b^{v_h, v_l} \mu_b^{\text{Proc}}) + o_b^{v_l} (r_{0, b}^{v_l} \alpha^{\text{BH}}). \quad (19) \end{aligned}$$

Furthermore, the cost of the access transmission resource usage for transferring the requested video file to user u is $\mathbb{S}_u^{\text{Cost,Ac}} = \sum_{b \in \mathcal{B}} \sum_{n \in \mathcal{N}} (p_{b,u}^n \alpha_b^{\text{Pow}} + \tau_{b,u}^n W_s \alpha_b^{\text{Sub}})$. Therefore, the cost of serving the request of user u for video v_l is $\mathbb{S}_u^{\text{Cost,User},v_l} = \delta_u^{v_l} \left(\mathbb{S}_u^{\text{Cost,Ac}} + \sum_{b \in \mathcal{B}} \theta_{b,u} \mathbb{S}_b^{\text{Cost,RRS},v_l} \right)$ which should be paid by slice m , if $u \in \mathcal{U}_m$. Hence, the revenue of each slice for serving video v_l to user $u \in \mathcal{U}_m$ is $\left(\sum_{b \in \mathcal{B}} r_{b,u}^{\text{Ac}} \psi_m - \mathbb{S}_u^{\text{Cost,User},v_l} \right)$.

Based on (2), each slice pays the cost of storage, processing, backhaul, and fronthaul resource usages for each video provisioning to each cell only once. Moreover, each slice m pays the usage cost of each subcarrier only once in each cell, even when the subcarrier is shared among users in \mathcal{U}_m in that cell via the MC-NOMA technology. Accordingly, the revenue of slice m in Phase 2 can be defined as

$$\begin{aligned} \mathbb{S}_m^{\text{slice}} &= \sum_{u \in \mathcal{U}_m} \sum_{b \in \mathcal{B}} r_{b,u}^{\text{Ac}} \psi_m - \sum_{u \in \mathcal{U}_m} \sum_{b \in \mathcal{B}} \sum_{n \in \mathcal{N}} (p_{b,u}^n \alpha_b^{\text{Pow}}) - \sum_{b \in \mathcal{B}} \sum_{n \in \mathcal{N}} \left(\max_{u \in \mathcal{U}_m} \{ \tau_{b,u}^n \} W_s \alpha_b^{\text{Sub}} \right) \\ &\quad - \sum_{b \in \mathcal{B}} \sum_{v_l \in \mathcal{V}} \min \left\{ \sum_{u \in \mathcal{U}_m} \theta_{b,u} \delta_u^{v_l}, 1 \right\} \mathbb{S}_b^{\text{Cost,RRS},v_l}. \quad (20) \end{aligned}$$

In Phase 2, with the objective of maximizing the total delivery revenue of slices denoted by $\mathbb{S}_{\text{tot}} = \sum_{m \in \mathcal{M}} \mathbb{S}_m^{\text{slice}}$ under the QoS requirements of users, we jointly optimize the user association, access transmit power and subcarrier allocation, fronthaul and backhaul rate adaption, processing resource allocation, and request scheduling to have an efficient delivery performance. For ease of notations, we denote $\boldsymbol{\theta} = [\theta_{b,u}]$, $\boldsymbol{\phi} = [\phi_b^{v_h, v_l}]$, $\boldsymbol{p} = [p_{b,u}^n]$, $\boldsymbol{\tau} = [\tau_{b,u}^n]$, $\boldsymbol{r}^{\text{BH}} = [r_{0,b}^{v_l}]$, $\boldsymbol{r}^{\text{FH}} = [r_{b',b}^{v_l}]$, $\boldsymbol{\Upsilon} = [\boldsymbol{x}, \boldsymbol{y}, \boldsymbol{z}, \boldsymbol{t}, \boldsymbol{w}, \boldsymbol{o}]$, $\boldsymbol{x} = [x_b^{v_l}]$, $\boldsymbol{y} = [y_b^{v_h, v_l}]$, $\boldsymbol{z} = [z_{b',b}^{v_l}]$, $\boldsymbol{t} = [t_{b',b}^{v_h, v_l}]$, $\boldsymbol{w} = [w_{b',b}^{v_h, v_l}]$, and $\boldsymbol{o} = [o_b^{v_l}]$. The delivery optimization problem can be formulated as

$$\max_{\boldsymbol{\theta}, \boldsymbol{\phi}, \boldsymbol{p}, \boldsymbol{\tau}, \boldsymbol{r}^{\text{BH}}, \boldsymbol{r}^{\text{FH}}, \boldsymbol{\Upsilon}} \mathbb{S}_{\text{tot}} \quad (21a)$$

s.t. (1)-(4), (6), (7)-(18),

$$y_b^{v_h, v_l} = 0, t_{b', b}^{v_h, v_l} = 0, w_{b', b}^{v_h, v_l} = 0, \forall h \leq l, \quad (21b)$$

$$\sum_{u \in \mathcal{U}} \tau_{b, u}^n \leq \Psi_b, \forall b \in \mathcal{B}, n \in \mathcal{N}, \quad (21c)$$

$$\theta_{b, u}, \tau_{b, u}^n, x_b^{v_l}, y_b^{v_h, v_l}, z_{b', b}^{v_l}, t_{b', b}^{v_h, v_l}, w_{b', b}^{v_h, v_l}, o_b^{v_l} \in \{0, 1\}, \phi_b^{v_h, v_l} \in \{0, 1, 2, \dots\}, p_{b, u}^n, r_{0, b}^{v_l}, r_{b', b}^{v_l} \geq 0, \quad (21d)$$

where (21c) represents that in each cell b , each subcarrier n can be assigned to at most Ψ_b users [17].

C. Phase 1

In this phase, we aim to design a DACPS by utilizing the delivery opportunities in Phase 2. Note that the users' request and CSI for Phase 2 are not available in this phase. To utilize the delivery model in the DACPS design, we need some stochastic information about videos popularity and wireless channel conditions. Similar to [3], [22], [32], [34], we assume that the VPD changes slowly compared to the instantaneous requests of users and remains fixed for the entirety of the network's operational time. Also, this parameter can be estimated by the operators by collecting prior set of requests of users [3], [32], [34]. Accordingly, we assume that VPD is available at the scheduler in Phase 1 and does not change during Phase 2, i.e., is valid for Phase 2. Similarly, the CDI can be averaged over various CSIs in different time slots of prior Phase 2 [3]. Assume that the VPD follows the Zipf distribution with the Zipf parameter λ and is the same among all users in the network [3], [22], [27]. Therefore, the popularity of requesting video v_l with rank⁶ Λ_{v_l} is given by $\Delta_{v_l} = \frac{1/(\Lambda_{v_l})^\lambda}{\sum_{v_l \in \mathcal{V}} 1/(\Lambda_{v_l})^\lambda}, \forall v_l \in \mathcal{V}$. To design a DACPS which covers the whole Phase 2, we propose an averaged based joint cache placement and ergodic resource allocation based on the VPD and CDI. Our DACPS is valid until the VPD and/or the CDI changes [3].

In Phase 1, we aim to formulate the stochastic problem of maximizing the total revenue of slices based on the available VPD and CDI to have an efficient delivery performance in Phase 2. In other words, since requests of users and CSI are not available in Phase 1, (21) should be reformulated based on the VPD and CDI. In this regard, the average or ergodic data rate of wireless access link between user u and RRS b is $\bar{r}_{b, u}^{\text{Ac}} = \mathbb{E}_{\mathbf{h}} \{r_{b, u}^{\text{Ac}}\}$, where $\mathbb{E}_{\mathbf{h}} \{\cdot\}$ is the

⁶Consider that the videos in \mathcal{V} are randomly sorted from 1 to VL .

expectation operator on the channel power gains [3]. This expectation is necessary even in slow fading scenarios, since the whole of Phase 2 has a much longer time length compared to Phase 1. In this phase, in contrast to the instantaneous access delays formulated in Subsection II-B, the average access delay for receiving video v_l from RRS b at user u obtained by $\bar{D}_{b,u}^{\text{Ac},v_l} = \frac{s_{v_l}}{\bar{r}_{b,u}^{\text{Ac}}}$ is considered. Moreover, in order to apply SIC, the average SIC constraint should be satisfied as⁷

$$\mathbb{E}_{\mathbf{h}} \left\{ \tau_{b,u}^n \frac{p_{b,u'}^n h_{b,u}^n}{\sum_{\substack{v \in \mathcal{U}, v \neq u' \\ h_{b,v}^n > h_{b,u'}^n}} p_{b,v}^n h_{b,u}^n + I_{b,u}^{\text{Inter},n} + \sigma_{b,u}^n} \right\} > \mathbb{E}_{\mathbf{h}} \{ \tau_{b,u'}^n \gamma_{b,u'}^n \}, \forall b \in \mathcal{B}, u, u' \in \mathcal{U}, n \in \mathcal{N},$$

$$\tau_{b,u}^n, \tau_{b,u'}^n > 0, \mathbb{E}_{\mathbf{h}} \{ h_{b,u}^n \} > \mathbb{E}_{\mathbf{h}} \{ h_{b,u'}^n \}. \quad (22)$$

Furthermore, since the requests of users ($\delta_u^{v_l} \in \{0, 1\}$) are unknown in Phase 1, constraint (2) should be reformulated based on the VPD ($\Delta^{v_l} \in [0, 1]$) which is non-achievable. To tackle this challenge and cover all possible situations in Phase 2, we assume that all videos should be served by each RRS based on one of the events described in Fig. 3 if at least one user is associated with that RRS. Hence, we have

$$x_b^{v_l} + \sum_{\substack{v_h \in \mathcal{V} \\ h > l}} y_b^{v_h, v_l} + \sum_{\substack{b' \in \mathcal{B} \\ b' \neq b}} z_{b', b}^{v_l} + \sum_{\substack{b' \in \mathcal{B} \\ b' \neq b}} \sum_{\substack{v_h \in \mathcal{V} \\ h > l}} (t_{b', b}^{v_h, v_l} + w_{b', b}^{v_h, v_l}) + o_b^{v_l} = \min \left\{ \sum_{u=1}^U \theta_{b,u}, 1 \right\}, \forall b \in \mathcal{B}, v_l \in \mathcal{V}. \quad (23)$$

Although this constraint consumes more physical resources, it covers all possible situations. In other words, it guarantees that various sets of arrival requests in different time slots of Phase 2 can be served [7]. With this assumption and available CDI, constraints (12), (13), (15), (17), and (18) in Phase 2 are reformulated as

$$y_b^{v_h, v_l} D_b^{\text{TC}, v_h, v_l} \leq \bar{D}_{b,u}^{\text{Ac}, v_l}, \quad z_{b', b}^{v_l} D_{b', b}^{\text{FH}, v_l} \leq \bar{D}_{b,u}^{\text{Ac}, v_l}, \quad t_{b', b}^{v_h, v_l} D_{b', b}^{\text{FH}, v_l} \leq \bar{D}_{b,u}^{\text{Ac}, v_l},$$

$$w_{b', b}^{v_h, v_l} D_b^{\text{TC}, v_h, v_l} \leq \bar{D}_{b,u}^{\text{Ac}, v_l}, \quad o_b^{v_l} D_{0,b}^{\text{BH}, v_l} \leq \bar{D}_{b,u}^{\text{Ac}, v_l}, \quad (24)$$

respectively. Let C_b^{max} be the maximum storage capacity of RRS b . In contrast to Phase 2, in this phase, we add a cache size constraint for each RRS as follows:

$$\sum_{v_l \in \mathcal{V}} \rho_b^{v_l} s_{v_l} \leq C_b^{\text{max}}, \forall b \in \mathcal{B}. \quad (25)$$

⁷In contrast to Phase 2 where the SIC of MC-NOMA is applied based on the CSI, in Phase 1, we apply SIC based on available CDI.

In Phase 1, our pricing model presented in Subsection II-B is also averaged based on both VPD and CDI. In this line, the average provisioning cost of a video file at RRS b can be formulated as $\bar{\mathbb{S}}_b^{\text{Cost,RRS}} = \sum_{v_l \in \mathcal{V}} \Delta_{v_l} \mathbb{S}_b^{\text{Cost,RRS},v_l}$. Moreover, the average reward of each slice m for providing a video file to user $u \in \mathcal{U}_m$ based on the considered average data rate $\bar{r}_{b,u}^{\text{Ac}}$ can be obtained by $\sum_{b \in \mathcal{B}} \bar{r}_{b,u}^{\text{Ac}} \psi_m$. Therefore, the average revenue of slice m is

$$\bar{\mathbb{S}}_m^{\text{slice}} = \sum_{u \in \mathcal{U}_m} \sum_{b \in \mathcal{B}} \bar{r}_{b,u}^{\text{Ac}} \psi_m - \sum_{u \in \mathcal{U}_m} \sum_{b \in \mathcal{B}} \sum_{n \in \mathcal{N}} (p_{b,u}^n \alpha_b^{\text{Pow}}) - \sum_{b \in \mathcal{B}} \sum_{n \in \mathcal{N}} \left(\max_{u \in \mathcal{U}_m} \{\tau_{b,u}^n\} W_s \alpha_b^{\text{Sub}} \right) - \sum_{b \in \mathcal{B}} f_{b,m}(\boldsymbol{\theta}) \bar{\mathbb{S}}_b^{\text{Cost,RRS}}, \quad (26)$$

where $f_{b,m}(\boldsymbol{\theta})$ is a function of $\theta_{b,u}$ which represents the number of specific videos in \mathcal{V} requested by users in \mathcal{U}_m associated with RRS b . The main challenge of (26) is obtaining an exact closed-form representation for $f_{b,m}(\boldsymbol{\theta})$ based on the available VPD which cannot be obtained, since the available VPD is independent from the user association process. Obviously, the value of $f_{b,m}(\boldsymbol{\theta})$ is upper-bounded by $\sum_{u \in \mathcal{U}_m} \theta_{b,u}$ and also is lower-bounded by $\min \left\{ \sum_{u \in \mathcal{U}_m} \theta_{b,u}, 1 \right\}$. Generally, the diversity of requesting video files affects $f_{b,m}(\boldsymbol{\theta})$. Specifically, if users have more diverse requests, i.e., $\lambda \rightarrow 0$, $f_{b,m}(\boldsymbol{\theta})$ increases which degrades the revenue of slices. Besides, if users have less diverse requests, i.e., $\lambda \rightarrow \infty$ or only a few video files are requested among all users, $f_{b,m}(\boldsymbol{\theta})$ decreases. Therefore, to obtain a closed-form representation for $f_{b,m}(\boldsymbol{\theta})$ in (26), we propose two low-diversity (LD) and high-diversity (HD) schemes. In the LD scheme, each slice assumes that all of its own users have the same requests based on the VPD. Hence, this scheme considers the best requesting situation which provides the maximum achievable revenue of slices. Conversely, in the HD scheme, each slice assumes that all of its users have different requests, i.e., the worst requesting situation is considered. To handle the different requesting diversity situations in the CPS design, we propose two baseline diversity CPSs, namely LD and HD. In the LD strategy, we consider the upper-bound value of the average revenue of each slice formulated as

$$\bar{\mathbb{S}}_m^{\text{slice,UB}} = \sum_{u \in \mathcal{U}_m} \sum_{b \in \mathcal{B}} \bar{r}_{b,u}^{\text{Ac}} \psi_m - \sum_{u \in \mathcal{U}_m} \sum_{b \in \mathcal{B}} \sum_{n \in \mathcal{N}} (p_{b,u}^n \alpha_b^{\text{Pow}}) - \sum_{b \in \mathcal{B}} \sum_{n \in \mathcal{N}} \left(\max_{u \in \mathcal{U}_m} \{\tau_{b,u}^n\} W_s \alpha_b^{\text{Sub}} \right) - \sum_{b \in \mathcal{B}} \min \left\{ \sum_{u \in \mathcal{U}_m} \theta_{b,u}, 1 \right\} \bar{\mathbb{S}}_b^{\text{Cost,RRS}}, \quad (27)$$

which is compatible with the LD scheme. On the other hand, for the HD strategy, we consider the lower-bound average revenue of each slice which is expressed as

$$\bar{\$}_m^{\text{slice, LB}} = \sum_{u \in \mathcal{U}_m} \sum_{b \in \mathcal{B}} \bar{r}_{b,u}^{\text{Ac}} \psi_m - \sum_{u \in \mathcal{U}_m} \sum_{b \in \mathcal{B}} \sum_{n \in \mathcal{N}} (p_{b,u}^n \alpha_b^{\text{Pow}}) - \sum_{b \in \mathcal{B}} \sum_{n \in \mathcal{N}} \left(\max_{u \in \mathcal{U}_m} \{\tau_{b,u}^n\} W_s \alpha_b^{\text{Sub}} \right) - \sum_{b \in \mathcal{B}} \sum_{u \in \mathcal{U}_m} \theta_{b,u} \bar{\$}_b^{\text{Cost, RRS}}. \quad (28)$$

This strategy is also compatible with the HD scheme. In this phase, we design DACPSs in the LD and HD schemes to maximize the total estimated average revenue of slices which are formulated as $\bar{\$}_{\text{tot}}^{\text{LD}} = \sum_{m \in \mathcal{M}} \bar{\$}_m^{\text{slice, UB}}$ and $\bar{\$}_{\text{tot}}^{\text{HD}} = \sum_{m \in \mathcal{M}} \bar{\$}_m^{\text{slice, LB}}$, respectively. The cache placement optimization problem in the LD scheme is

$$\max_{\rho, \theta, \phi, p, \tau, r^{\text{BH}}, r^{\text{FH}}, \Upsilon} \bar{\$}_{\text{tot}}^{\text{LD}} \quad (29a)$$

$$\text{s.t. (1), (3), (4), (7)-(10), (14), (16), (21b)-(21d), (22)-(24),}$$

$$\sum_{b \in \mathcal{B}} \bar{r}_{b,u}^{\text{Ac}} \geq R_m^{\text{min}}, \forall m \in \mathcal{M}, u \in \mathcal{U}_m, \quad (29b)$$

$$\rho_b^{vl} \in \{0, 1\}. \quad (29c)$$

The cache placement optimization problem in the HD scheme is

$$\max_{\rho, \theta, \phi, p, \tau, r^{\text{BH}}, r^{\text{FH}}, \Upsilon} \bar{\$}_{\text{tot}}^{\text{HD}} \quad (30a)$$

$$\text{s.t. (1), (3), (4), (7)-(10), (14), (16), (21b)-(21d), (22)-(24), (29b), (29c).}$$

Table II summarizes the main notations used in each phase.

The mixed-integer nonlinear programming (MINLP) problems (21), (29), and (30) are completely NP-hard which is mathematically proved in [37] in the transmit power and subcarrier allocation problem for MC-NOMA in order to maximize the downlink data rate of users. In addition, in [38], it is mentioned that data rate maximization optimization problems with interferences are completely NP-hard for OFDMA-based wireless networks and it is non-achievable to find the global optimum joint transmit power and subcarrier allocation policy by any existing method. Since the transmit power and subcarrier allocation in OFDMA is a special case of MC-NOMA [37], the result follows. The exhaustive search requires the examination of all $(2S^{\text{Power}})^{BUN} \cdot (2S^{\text{FH}})^{B^2VL} \cdot (8S^{\text{BH}})^{BVL} \cdot (2S^{\text{Process}})^{BVL^2} \cdot 2^{BU} \cdot 4^{B^2VL^2}$ possible situations where S^{Power} , S^{FH} , S^{BH} , and S^{Process} are the number of values that each variable in p , r^{FH} , r^{BH} , and ϕ can take, respectively. Accordingly, it is very challenging and impractical to find the global

TABLE II: Main notations.

Description	Notation	Phase	Description	Notation	Phase
Number of users	U	1 & 2	Number of RRSs	B	1 & 2
Number of slices	M	1 & 2	Number of unique videos	V	1 & 2
Number of bitrate variants	L	1 & 2	The v^{th} video type with the l^{th} bitrate variant	v_l	1 & 2
Size of video v_l	s_{v_l}	1 & 2	Request of user u for video v_l	$\delta_{b,u}^{v_l}$	2
User association indicator	$\theta_{b,u}$	1 & 2	Scheduling events	$(x_b^{v_l}, y_b^{v_l}, z_{b',b}^{v_l}, u_{b',b}^{v_l}, o_b^{v_l})$	1 & 2
Cache placement indicator	$\rho_b^{v_l}$	1 & 2	Number of subcarriers	N	1 & 2
Subcarrier assignment indicator	$\tau_{b,u}^n$	1 & 2	Transmit power	$p_{b,u}^n$	1 & 2
Instantaneous channel power gain	$h_{b,u}^n$	2	Instantaneous SINR	$\gamma_{b,u}^n$	2
Subcarrier bandwidth	W_c	1 & 2	Instantaneous data rate	$r_{b,u}^n$	2
AWGN noise power	$\sigma_{b,u}^n$	1 & 2	Instantaneous data rate	$r_{b,u}^n$	2
Maximum transmit power of each RRS	P_b^{\max}	1 & 2	Instantaneous access latency	$D_{b,u}^{\text{Ac},v_l}$	2
Size of transcoding task	η^{v_h, v_l}	1 & 2	Workload of each transcoding task	$N_{\text{Cycle}}^{v_h, v_l}$	1 & 2
Processing resource of each task	$\phi_b^{v_h, v_l}$	1 & 2	Maximum processing capacity of each RRS	χ_b^{\max}	1 & 2
Transcoding delay	$D_b^{\text{TC}, v_h, v_l}$	1 & 2	Backhaul capacity for each video	$r_{0,b}^{v_l}$	1 & 2
Fronthaul capacity for each video	$r_{b',b}^{v_l}$	1 & 2	Maximum capacity of each backhaul link	$R_{b',b}^{\max}$	1 & 2
Maximum capacity of each fronthaul link	$R_{b',b}^{\max}$	1 & 2	Backhaul delay	$D_{0,b}^{\text{BH}, v_l}$	1 & 2
Fronthaul delay	$D_{b',b}^{\text{FH}, v_l}$	1 & 2	Contracted minimum data rate at each slice	$R_{v_m}^{\min}$	1 & 2
Unit price of transmit power	α_b^{Pow}	1 & 2	Unit price of subcarrier	α_b^{Sub}	1 & 2
Unit price of backhaul capacity	α^{BH}	1 & 2	Unit price of fronthaul capacity	α^{FH}	1 & 2
Unit price of storage	μ_b^{Cache}	1 & 2	Unit price of processing	μ_b^{Proc}	1 & 2
Unit reward of each slice	ψ_{v_m}	1 & 2	Provisioning cost of each video at each slice	$\mathcal{C}_b^{\text{Cost}, \text{RRS}, v_l}$	2
Revenue of each slice	$\mathcal{R}_m^{\text{slice}}$	2	Total revenue of slices	\mathcal{R}_{tot}	2
Total revenue of slices	\mathcal{R}_{tot}	2	Maximum number of each user for each subcarrier	Ψ_b	1 & 2
Popularity of requesting videos	Δ_{v_l}	1	Average rate of each user	$\bar{r}_{b,u}^{\text{Ac}}$	1
Average latency at each user	$D_{b,u}^{\text{Ac}, v_l}$	1	Maximum storage capacity of each RRS	C_b^{max}	1
Average provisioning cost of a video file at each RRS	$\bar{\mathcal{C}}_b^{\text{Cost}, \text{RRS}}$	1	Average revenue of each slice	$\mathcal{R}_m^{\text{slice}}$	1
Number of videos requested by users in \mathcal{U}_m associated with RRS b	$f_{b,m}(\theta)$	1	Upper-bound of total average revenue of slices	$\mathcal{R}_{\text{tot}}^{\text{LD}}$	1
Lower-bound of total average revenue of slices	$\mathcal{R}_{\text{tot}}^{\text{LD}}$	1	-	-	-

optimum solution for such large-scale and NP-hard optimization problems, since the number of optimization variables and constraints grow exponentially [22], [24]–[26], [37].

The main structure of optimization problems (21) and (29) are the same for a fixed placement variable ρ . Therefore, we provide a local optimum resource allocation algorithm that can be adopted for both problems (21) and (29). However, (30) and (29) differ in objective function. Accordingly, we modify the solution algorithm proposed for (29) to be applied to (30).

III. DELIVERY-AWARE COOPERATIVE MULTI-BITRATE VIDEO CACHING AND TRANSCODING ALGORITHMS

This section provides solution algorithms for the main problems (21), (29) and (30).

A. DACPSs and Delivery Algorithm

Here, we propose an efficient solution algorithm for (29) by utilizing the alternate optimization algorithm [4], [36], [38]. This algorithm consists of two main steps: 1) finding joint \mathbf{p} , ϕ , \mathbf{r}^{FH} ,

Algorithm 1 The main alternate method.

- 1: Initialize $\Upsilon_0, \rho_0, \mathbf{p}_0, \phi_0, \mathbf{r}_0^{\text{FH}}, \mathbf{r}_0^{\text{BH}}, \tau_0$, and θ_0 .
 - repeat**
 - 2: **for** $\kappa_1 = 1$ to Γ_1 **do**
 - 3: **Step 1:** Find $(\mathbf{p}_{\kappa_1}, \phi_{\kappa_1}, \mathbf{r}_{\kappa_1}^{\text{FH}}, \mathbf{r}_{\kappa_1}^{\text{BH}})$ by solving (29) for a fixed $(\Upsilon_{\kappa_1-1}, \rho_{\kappa_1-1}, \tau_{\kappa_1-1}, \theta_{\kappa_1-1})$.
 - 4: **Step 2:** Find $(\Upsilon_{\kappa_1}, \rho_{\kappa_1}, \tau_{\kappa_1}, \theta_{\kappa_1})$ by solving (29) for a given $(\mathbf{p}_{\kappa_1}, \phi_{\kappa_1}, \mathbf{r}_{\kappa_1}^{\text{FH}}, \mathbf{r}_{\kappa_1}^{\text{BH}})$.
 - 5: **Until** $|\bar{\mathcal{S}}_{\text{tot}}^{\text{LD}}(\kappa_1) - \bar{\mathcal{S}}_{\text{tot}}^{\text{LD}}(\kappa_1 - 1)| \leq \varepsilon_1$ or $\kappa_1 = \Gamma_1$.
 - 6: Set $\kappa_1 = \kappa_1 + 1$.
 - 7: **end for**
 - 8: $\Upsilon_{\kappa_1}, \rho_{\kappa_1}, \mathbf{p}_{\kappa_1}, \phi_{\kappa_1}, \mathbf{r}_{\kappa_1}^{\text{FH}}, \mathbf{r}_{\kappa_1}^{\text{BH}}, \tau_{\kappa_1}$, and θ_{κ_1} are adopted for the network.
-

and \mathbf{r}^{BH} ; 2) finding joint Υ, ρ, τ , and θ . We repeat the aforementioned steps until we have $|\bar{\mathcal{S}}_{\text{tot}}^{\text{LD}}(\kappa_1) - \bar{\mathcal{S}}_{\text{tot}}^{\text{LD}}(\kappa_1 - 1)| \leq \varepsilon_1$ where ε_1 is a positive small value and κ_1 is the iteration index, or the number of main iterations exceeds a pre-defined threshold Γ_1 . The proposed approach is summarized in Algorithm 1.

1) *Step 1:* In the first step, we obtain $\mathbf{p}, \phi, \mathbf{r}^{\text{FH}}$ and \mathbf{r}^{BH} jointly, by solving the following subproblem for fixed Υ, ρ, τ , and θ as

$$\max_{\phi, \mathbf{p}, \mathbf{r}^{\text{BH}}, \mathbf{r}^{\text{FH}}} \bar{\mathcal{S}}_{\text{tot}}^{\text{LD}} \quad (31a)$$

$$\text{s.t. (7)-(10), (14), (16), (21d), (22), (24), (29b).}$$

Problem (31) is still MINLP, which is NP-hard, due to non-concavity of objective function (31a) and non-convexity of constraints (14), (16), (21d), (22), (24), and (29b). In order to deal with the aforementioned challenges, we first relax $\phi_b^{v_h, v_l}$ in (21d) to be a non-negative real value [10], [13], which is an acceptable approach in this context since the maximum number of CPU cycles in each processor is on the order of 10^9 [11]–[13]. For the non-convex constraints, we apply transformation methods to tackle their non-convexity (please see Appendix A). Then, to tackle the non-concavity of $\bar{r}_{b,u}^{\text{Ac}}$ in (31a) and (29b), and its non-convexity in constraints (34e)–(34i) of the transformed problem (presented in Appendix A), we use the successive convex approximation (SCA) approach based on the difference-of-two-concave-functions (D.C.) approximation method [32], [38], [39]. In this regard, we first initialize the approximation parameters. Then, we solve

Algorithm 2 The proposed SCA algorithm with the D.C. approximation method.

- 1: Initialize \mathbf{p}_0 .
 - repeat**
 - 2: Update the convex approximated forms of (29b), (34e)-(34i) and substitute them into (34).
 - 3: Find $(\phi_{\kappa_2}, \mathbf{p}_{\kappa_2}, \mathbf{r}_{\kappa_2}^{\text{BH}}, \mathbf{r}_{\kappa_2}^{\text{FH}})$ by solving the convex approximated problem of (34).
 - 4: Set $\kappa_2 = \kappa_2 + 1$
 - Until** Convergence of \mathbf{p} .
 - 5: The variables \mathbf{p} , \mathbf{r}^{BH} , \mathbf{r}^{FH} , and ϕ are the outputs of the algorithm.
-

the convex approximated problem to find $(\phi, \mathbf{p}, \mathbf{r}^{\text{BH}}, \mathbf{r}^{\text{FH}})$. These iterations are repeated until the stopping criterion is satisfied. The derivations of the proposed SCA algorithm are presented in Appendix B. Additionally, the pseudo code of the SCA algorithm with the D.C. approximation method is summarized in Algorithm 2.

2) *Step 2*: Here, we jointly find the binary variables Υ , ρ , θ , and τ for the given $(\mathbf{p}, \phi, \mathbf{r}^{\text{FH}}, \mathbf{r}^{\text{BH}})$ by solving the following subproblem:

$$\begin{aligned} \min_{\Upsilon, \rho, \theta, \tau} \quad & \bar{\$}_{\text{tot}}^{\text{LD}} & (32a) \\ \text{s.t.} \quad & (1), (3), (4), (8)-(10), (14), (16), (21b)-(21d), (22)-(24), (29b), (29c). \end{aligned}$$

Problem (32) is classified as integer nonlinear programming (INLP) due to combinatorial constraints (21d) with respect to Υ , θ , and τ , combinatorial constraints in (29c) with respect to ρ , nonlinear SIC constraint (22) with respect to τ , the term $\min\{\sum_{u=1}^U \theta_{b,u}, 1\}$ in (23), both the terms $\max_{u \in \mathcal{U}_m} \{\tau_{b,u}^n\}$ and $\min\{\sum_{u \in \mathcal{U}_m} \theta_{b,u}, 1\}$ in (32a) (please refer to (27)), multiplication of $\min\{\sum_{u \in \mathcal{U}_m} \theta_{b,u}, 1\}$ in scheduling variables in Υ in (32a) (please refer to (27) and (19)), nonlinearity of fractional delay functions in (14) and (16), and average access delay functions in (24) with respect to τ . To solve (32), our aim is to transform (32) into an integer disciplined convex programming (IDCP). This can be easily solved by utilizing the efficient standard optimization software CVX with the internal solver MOSEK that applies the Branch&bound&cut algorithm [3], [17], [39]–[41].

Proposition 1: The INLP problem (32) can be equivalently transformed into an IDCP form which is presented in Appendix C.

To solve (21) for Phase 2, we can also apply Algorithm 1, since when ρ is fixed, (21) and (29) have a similar structure. Due to space limitations, the solution for the problem of Phase 2 is not included here. To solve (30) in the HD scheme, we again apply a similar method to Algorithm 1 (See Appendix D).

B. Convergence of The Proposed Algorithms

Here, we discuss the convergence of our proposed Algorithm 1 for solving (29). This discussion is presented in the format of the following two propositions.

Proposition 2: The objective function (29a) is upper-bounded by the total average reward of slices which is obtained by $\sum_{u \in \mathcal{U}_m} \sum_{b \in \mathcal{B}} \bar{r}_{b,u}^{\text{Ac}} \psi_m$ that is a nonnegative finite term, due to limited access bandwidth and constraint (7). Therefore, for a feasible problem (29), the proposed alternate Algorithm 1 will converge to a locally optimal solution.

Proof. Please see Appendix E. □

Proposition 3: The SCA approach with the D.C. approximation method generates a sequence of improved feasible solutions. Therefore, the proposed algorithm for solving (31) will converge to a locally optimal solution when the number of SCA iterations are large enough.

Proof. Please see Appendix F. □

Since all proposed algorithms have similar structures, the convergence of the other algorithms can be proved same as the proposed Algorithm 1 for solving (29).

C. Computational Complexity of the Proposed Algorithm

Here, we aim to obtain the computational complexity of the proposed solution algorithms for problems (21), (29), and (30). Since the proposed alternate algorithms for solving (21), (29), and (30) have basically the same structure, we only present the details of obtaining the computational complexity of solving (29) using Algorithm 1. After that, the computational complexity of solving (21) and (30) is investigated.

In the first step of Algorithm 1, we first use a transformation method presented in Appendix A to solve (31). We then solve the equivalent result problem (34) using the iterative SCA approach based on the D.C. approximation method. In each iteration κ_2 of SCA, the approximated disciplined convex programming (DCP) problem of (34) is solved by CVX, which employs

the geometric programming with the interior-point method (IPM) [39], [40]. Therefore, the computational complexity of solving the approximated problem of (34) is on the order of $\Omega_{LD}^1 = \frac{\log(T_{LD}^1/(t^0 \varrho))}{\log \epsilon^0}$, where $T_{LD}^1 = 3B + B^2 + U + M + BU^2N + BVL(1 + B + L) + B^2VL^2(2 + 2U)$ is the total number of constraints in the approximated problem of (34), t^0 is the initial point for approximating the accuracy of the IPM, $0 < \varrho \ll \infty$ is the stopping criterion for the IPM, and ϵ^0 is for updating the accuracy of the IPM [39], [40]. Note that Ω_{LD}^1 is only for one iteration of the SCA approach. The total complexity of solving (34) by using the SCA method mainly depends on the number of optimization variables, constraints, and accuracy of the algorithm. In the second step of Algorithm 1, we find $(\Upsilon, \rho, \theta, \tau)$ by solving (32). In fact, we transform (32) into an equivalent IDCP problem (44) using the epigraph technique. The resulting IDCP problem (44) is also solved by utilizing CVX with the MOSEK solver. The complexity of solving (44) can thus be obtained by $\Omega_{LD}^2 = \frac{\log(T_{LD}^2/(t^0 \varrho))}{\log \epsilon^0}$, where $T_{LD}^2 = 3B + 2U + M + B^2 + 2BU + BN + 2BUN + BU^2N + BVL(2 + B + L + 6M + 4UN + 3LM + 3BM + 4LUN + 4BUN) + B^2VL^2(4 + 6M + 8UN)$ is the total number of constraints in (44). Accordingly, the total computational complexity of solving (29) is on the order of $\Omega_{LD}^{\text{tot}} = \Xi^{\text{Main}} (\Xi^{\text{SCA}} \Omega_{LD}^1 + \Omega_{LD}^2)$ where Ξ^{Main} and Ξ^{SCA} are the total number of main and SCA iterations, respectively.

The computational complexity of solving the cache placement optimization problem (30) can also be obtained using the same method as (29). In this line, the complexity of finding joint \mathbf{p} , ϕ , \mathbf{r}^{FH} and \mathbf{r}^{BH} at each iteration of the SCA approach is on the order of $\Omega_{\text{HD}}^1 = \frac{\log(T_{\text{HD}}^1/(t^0 \varrho))}{\log \epsilon^0}$, where T_{HD}^1 is exactly equal to T_{LD}^1 . On the other hand, the complexity of solving the second step of the proposed alternate algorithm for solving (30) is given by $\Omega_{\text{HD}}^2 = \frac{\log(T_{\text{HD}}^2/(t^0 \varrho))}{\log \epsilon^0}$, where $T_{\text{HD}}^2 = 3B + 2U + M + B^2 + BU + BN + 2BUN + BU^2N + BVL(2 + B + L + 6U + 4UN + 3LU + 3BU + 4LUN + 4BUN) + B^2VL^2(4 + 6U + 8UN)$.

The complexity of solving (21) can be obtained as the same way of obtaining the complexity of solving (29), since both the proposed algorithms have the same structure for a fixed ρ . In this way, the complexity of solving (21) and finding \mathbf{p} , ϕ , \mathbf{r}^{FH} and \mathbf{r}^{BH} is exactly on the order of Ω_{LD}^1 . Moreover, the computational complexity of finding (Υ, θ, τ) is obtained by $\Omega_{\text{Del}}^2 = \frac{\log(T_{\text{Del}}^2/(t^0 \varrho))}{\log \epsilon^0}$, where $T_{\text{Del}}^2 = 2B + 2U + M + B^2 + 2BU + BN + 2BUN + BU^2N + BVL(2 + B + L + 6M + 4UN + 3LM + 3BM + 4LUN + 4BUN) + B^2VL^2(4 + 6M + 8UN)$.

D. Designing a Low-Complexity Resource Allocation Framework

It is very important that the central scheduler be fast enough to readopt the delivery policy in each time slot of Phase 2 based on the arrival of instantaneous requests from users and CSI, especially in realistic ultra dense 5G wireless networks with a large number of unique videos. For this reason, we propose here another RAF that has a lower computational complexity in each time slot of Phase 2 than that of our proposed RAF in Fig. 2. The main part of the complexity of the proposed framework in Fig. 2 is caused by reallocating the radio resources as well as reassociating users to RRSs at each time slot of Phase 2 to readopt the access transmission strategy based on the arrival requests and CSI. However, some environments with higher path loss heavily limit the flexibility of the user association process and reduce the impact of the wireless small-scale fading on the SINR of users. On the other hand, we aim to utilize the benefits of radio resource allocation and user association policies in the MC-NOMA system to improve user data rates and correspondingly improve user revenues. Thus, in this novel framework, we adapt the obtained radio resource allocation, i.e., transmit power and subcarrier allocation, and user association policies in Phase 1 to all time slots of Phase 2. Hence, the system only reallocates the processing, fronthaul and backhaul resources as well as the request scheduling at the beginning of each time slot of Phase 2 based on the arrival requests from users. Accordingly, in this framework, the LD and HD cache placement problems are exactly the same as (29) and (30) whereas the delivery optimization problem at each time slot of Phase 2 is formulated as

$$\begin{aligned} & \max_{\phi, \mathbf{r}^{\text{BH}}, \mathbf{r}^{\text{FH}}, \Upsilon} \mathcal{S}_{\text{tot}} & (33a) \\ & \text{s.t. } (2), (3), (8)-(10), (12)-(18). \end{aligned}$$

The optimization problem (33) is a MINLP which can be efficiently solved by utilizing an alternate algorithm in which (33) is divided into two subproblems as: 1) finding joint ϕ , \mathbf{r}^{BH} , and \mathbf{r}^{FH} ; 2) finding Υ . The problem of finding joint ϕ , \mathbf{r}^{BH} , and \mathbf{r}^{FH} is a linear programming (LP) and thus, the globally optimal solution can be found by utilizing the CVX software or the Lagrange dual method. On the other hand, the IDCP problem of finding Υ is solved by using the MOSEK solver.

The computational complexity of solving (33) can be obtained as the same way of obtaining the complexity of solving (21). In this way, the complexity of finding ϕ , \mathbf{r}^{BH} , and \mathbf{r}^{FH} is on the order of $\Omega_{\text{Del,LowComplex}}^1 = \frac{\log(T_{\text{Del,LowComplex}}^1 / (t^0 \varrho))}{\log \epsilon^0}$, where $T_{\text{Del,LowComplex}}^1 = 2B + B^2 + BVL(1 +$

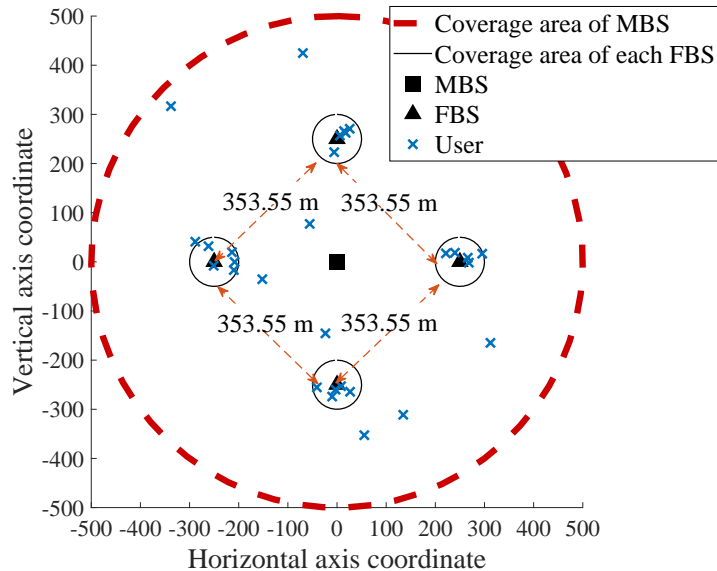


Fig. 4: Network setup and user placement in the simulation results.

$B + L) + 4B^2VL^2$. Moreover, the complexity of finding Υ is obtained by $\Omega_{\text{Del,LowComplex}}^2 = \frac{\log(T_{\text{Del,LowComplex}}^2 / (t^0 \varrho))}{\log \epsilon^0}$, where $T_{\text{Del,LowComplex}}^2 = 2B + B^2 + BVL(3 + 2B + 2L) + 6B^2VL^2$.

IV. SIMULATION RESULTS

In this section, we present simulation results that demonstrate the performance of our proposed CPSs via MATLAB Monte Carlo simulations through 500 network realizations [19]. The network topology and user placement is shown in Fig. 4 where a single high-power RRS (HP-RRS), i.e., MBS, is located in the center of a circular area with radius 500 m and 4 low-power RRSs (LP-RRS), i.e., FBS, are located in a distance of 250 m from the HP-RRS [38]. Ten users are uniformly deployed in the coverage area of HP-RRS while 5 users are located in the coverage area of each LP-RRS with radii of 50 m [38]. As seen in Fig. 4, the shortest distance from a FBS to another FBS is $250\sqrt{2} \approx 353.55$ m.

The wireless channel is centered at a frequency of 2.5 GHz with bandwidth $W = 5$ MHz, $N = 64$ and $W_s = 78.125$ KHz [35]. The combined path loss and shadowing is modeled as $128.1 + 37.6 \log_{10} d_{b,u} + z_{b,u}$ in dB in which $z_{b,u}$ is a log-normal shadowing random variable with the standard deviation of 8 dB, and $d_{b,u} > 0$ denotes the distance between RRS b and user u in km [5], [36], [42]. The small-scale fading of the wireless channel is modeled as independent and identically distributed Rayleigh fading with variance 1 [36]. The CDI is averaged over 1000

CSI samples for a fixed channel power loss, since the location of users and RRSs are fixed in our numerical examples. The PSD of AWGN noise is set to $N_0 = -174$ dBm/Hz with a noise figure of 9 dB at each user [23]. In the MC-NOMA technology, we set $\Psi_b = 2, \forall b \in \mathcal{B}$ [17], [35], [36]. For the HP-RRS, we set $P_1^{\max} = 47$ dBm whereas for each LP-RRS b , $P_b^{\max} = 27$ dBm [38].

We assume that there exists $V = 10$ unique videos, each having $L = 4$ bitrate variants. In our simulations, we set the relative bitrates of the four variants to be 0.45, 0.55, 0.67, and 0.82 of the original video bitrate 2 Mbps (HD quality) [6], [7]. Besides, all video variants have equal length of 10 minutes [7]. The skew parameter of the Zipf distribution is set to $\lambda = 0.8$ [6], [7]. Similar to [6], [7] we assume that the processing workload η^{v_h, v_l} is proportional to s_{v_l} . In this regard, we set $\eta^{v_h, v_l} = s_{v_l}$ [7].

For the proposed virtualization model, we assume that there exists $M = 2$ slices in the infrastructure with $R_1^{\min} = 1$ Mbps and $R_2^{\min} = 2$ Mbps. Each slice also has $U/2 = 15$ users such that each user subscribes to any slices with a probability of $1/M = 50\%$ [18], [19]. In our proposed pricing scheme, we take $\mu_1^{\text{Cache}} = 2$ units/Gbit, $\mu_b^{\text{Cache}} = 1.6$ units/Gbit, $\forall b \in \mathcal{B}/\{1\}$ [19], $\mu_1^{\text{Proc}} = 0.8$ units/GHz, $\mu_b^{\text{Proc}} = 0.7$ units/GHz, $\forall b \in \mathcal{B}/\{1\}$, $\alpha_1^{\text{Pow}} = 6$ units/Watt, $\alpha_b^{\text{Pow}} = 4$ units/Watt, $\forall b \in \mathcal{B}/\{1\}$, $\alpha_1^{\text{Sub}} = 60$ units/MHz, $\alpha_b^{\text{Sub}} = 40$ units/MHz, $\forall b \in \mathcal{B}/\{1\}$ [19], [30], $\alpha^{\text{FH}} = 2$ units/Mbps, $\alpha^{\text{BH}} = 5$ units/Mbps [30]. Moreover, the unit reward of slices are $\psi_1 = 8.75$ units/Mbps and $\psi_2 = 9$ units/Mbps [18], [19], [30].

For processing capacities, we set $\chi_1^{\max} = 50$ GHz (maximum number of CPU cycles per seconds in HP-RRS is 50×10^9) and $\chi_b^{\max} = 25$ GHz, $\forall b \in \mathcal{B}/\{1\}$. Moreover, the required number of CPU cycles per byte at each RRS b is set to $N_{\text{Cycle}}^{v_h, v_l} = 5900$ [11], [43]. For the storage capacities, we set $C_1^{\max} = 0.2 \sum_{v_l \in \mathcal{V}} s_{v_l}$ and $C_b^{\max} = 0.1 \sum_{v_l \in \mathcal{V}} s_{v_l}, \forall b \in \mathcal{B}/\{1\}$. For the fronthaul and backhaul capacities, we set $R_{b', b}^{\max} = 40$ Mbps and $R_{0, b}^{\max} = 80$ Mbps, respectively. The simulation settings are summarized in Table III.

To investigate the benefits of each technology in the system, we compare the CVCT system according to the following schemes: 1) No Caching (NC), where the storage and processing capacity of RRSs are equal to zero [23], [32]; 2) Non-Cooperative (NoCoop), where there is no cooperation between RRSs; 3) Cooperative Caching with No Transcoding (CCNT), where only the cooperative caching technology is considered for RRSs and the processing capacity of all RRSs are equal to zero; 4) The OMA technology (OMA), where the OFDMA technology is used for the downlink transmission of wireless access channels.

TABLE III: Simulation settings.

Description	Notation	Value	Description	Notation	Value
System Parameters			Virtualization and Pricing Parameters		
Carrier frequency	\times	2.5 GHz	Number of slices	M	2
Wireless channel bandwidth	W	5 MHz	Number of users of each slice	\times	15
Number of subcarriers	N	64	User selection distribution	\times	Uniform
Subcarrier bandwidth	W_c	78.125 KHz	Unit price of transmit power	α_b^{Pow}	HP-RRS: 6 units/Watt, LP-RRS: 4 units/Watt
Path loss model	\times	$128.1 + 37.6 \log_{10} d_{b,u} + z_{b,u}$ (dB), $d_{b,u}$ (Km)	Unit price of subcarrier bandwidth	α_b^{Sub}	HP-RRS: 60 units/MHz, LP-RRS: 40 units/MHz
Shadowing standard deviation	$z_{b,u}$	8 dB	Unit price of storage resources	μ_b^{Cache}	HP-RRS: 2 units/Gbit, LP-RRS: 1.6 units/Gbit
Small-scale fading model	\times	Rayleigh fading with variance 1	Unit price of processing resources	μ_b^{Proc}	HP-RRS: 0.8 units/GHz, LP-RRS: 0.7 units/GHz
PSD of AWGN	N_0	-174 dBm/Hz	Unit price of fronthaul capacity	α^{FH}	2 units/Mbps
Noise figure at users	\times	9 dB	Unit price of backhaul capacity	α^{BH}	5 units/Mbps
Video Parameters			Unit reward of slices	ψ_m	$\psi_1 = 8.75$ units/Mbps and $\psi_2 = 9$ units/Mbps
Number of unique videos	V	10	Threshold Parameters		
Number of bitrate variants	L	4	Transmit power of RRSs	P_b^{max}	HP-RRS: 47 dBm, LP-RRS: 27 dBm
Original video bitrate	\times	2 Mbps (HD quality)	Processing capacity of RRSs	χ_b^{max}	HP-RRS: 50 GHz, LP-RRS: 25 GHz
Relative bitrates	\times	[0.45, 0.55, 0.67, 0.82]	Storage capacity of RRSs	C_b^{max}	HP-RRS: 20%, LP-RRS: 10%
Video length	\times	10 minutes	Maximum fronthaul capacity	$R_{b',b}^{\text{max}}$	40 Mbps
Zipf parameter	λ	0.8	Maximum backhaul capacity	$R_{0,b}^{\text{max}}$	80 Mbps
Task workload	$N_{\text{Cycle}}^{\text{VH,VI}}$	5900	Maximum number of NOMA users	Ψ_b	2
Size of transcoding task	$\eta^{\text{Vh,VI}}$	s_{v_l}	Minimum data rate of each slice	R_m^{min}	$R_1^{\text{min}} = 1$ Mbps, $R_2^{\text{min}} = 2$ Mbps

We also compare the performance of our proposed DACPSs in each scheme with two conventional baseline popular/bitrate CPSs: 1) Most Popular Video (MPV), where each RRS caches the most popular videos until its storage is full [23], [32]; 2) High-Bitrate Video (HBV), where each RRS caches the high-bitrate variants of video files randomly until its storage is full.

As noted previously, obtaining the globally optimal solution of each cache placement and delivery optimization problem via the exhaustive search method would take an unrealistically long time for $U = 30$, $N = 64$, $B = 5$, and $VL = 40$ [32]. Thus, we limit our simulations to only evaluate the performance of our proposed solution algorithms. We also investigate the delivery performance gain achieved by each of our proposed RAF in terms of total delivery revenue of slices and computational complexity of the delivery algorithm.

A. Convergence of the Delivery Algorithm

Fig. 5 demonstrates the convergence of the proposed delivery algorithm for different CPSs. As shown, for all heuristic and the LD and HD strategies, the proposed delivery algorithm converge to stable values in maximum 6 iterations. In this figure, the dash lines refer to the upper-bound solutions when the algorithm converges. From Fig. 5, it can be seen that after 3 iterations, the proposed approach will achieve up to 95% of its upper-bound value for different CPSs which ensures us the proposed algorithm can be applied in practical scenarios in multiuser HV-MECs.

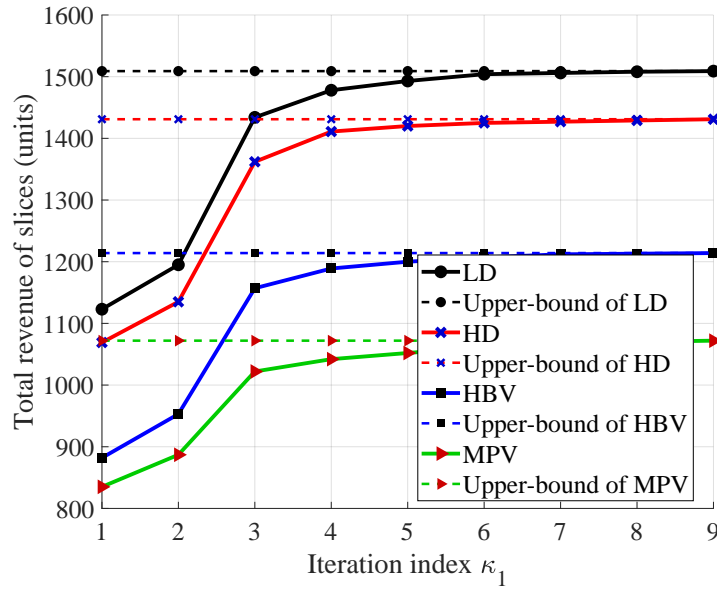
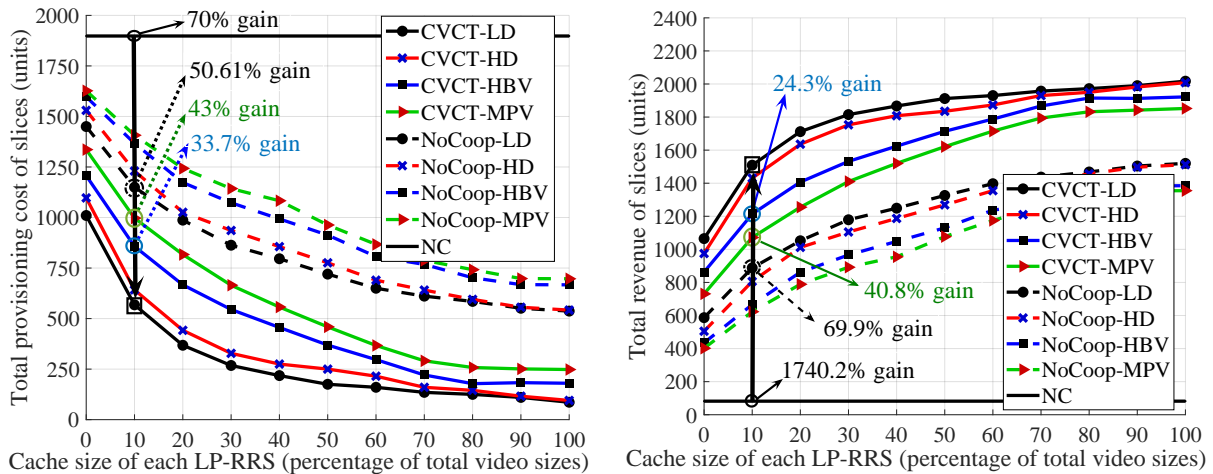


Fig. 5: The convergence in terms of total revenue of slices over the number of main iterations.

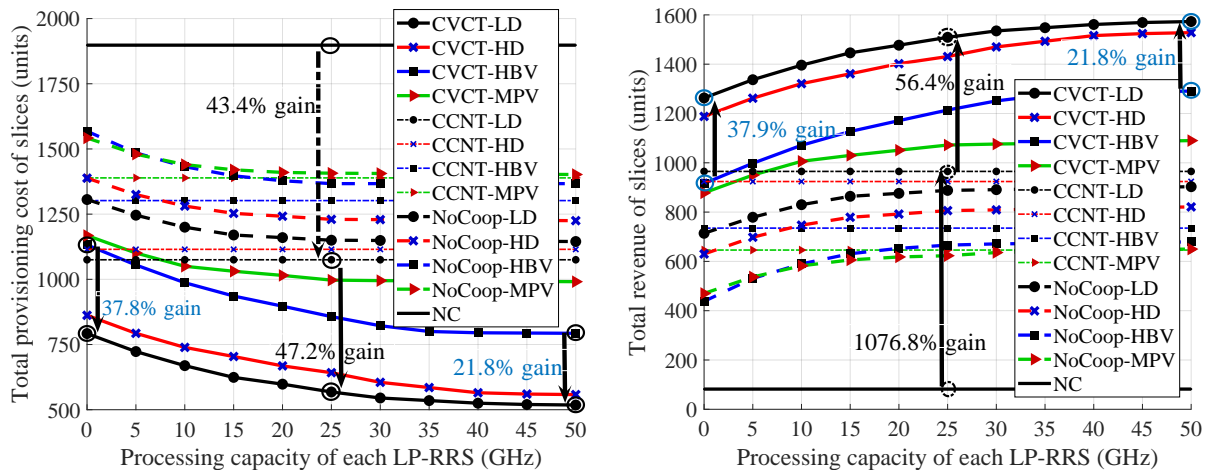


(a) Total provisioning cost of slices vs. storage capacity of LP-RRSs. (b) Total revenue of slices vs. storage capacity of LP-RRSs.

Fig. 6: Impact of storage capacity of LP-RRSs on the performance of CPSs in different schemes.

B. Impact of the Storage, Processing, and Fronthaul Capacities

1) *Impact of the storage capacity of RRSs*: In Fig. 6, we investigate the impact of storage capacity limitation at LP-RRSs on the performance of CPSs in cooperative and non-cooperative schemes. As expected, more storage capacities lead to more stored videos, which increases the cache hit ratio and subsequently provides more transcoding and cooperative communication



(a) Total provisioning cost of slices vs. processing capacity of LP-RRSs. (b) Total revenue of slices vs. processing capacity of LP-RRSs.

Fig. 7: Impact of processing capacity of LP-RRSs on the performance of CPSs in different schemes.

opportunities. Therefore, backhaul resource usage is significantly reduced, which decreases the total provisioning cost of slices (see Fig. 6(a)) and correspondingly improves the total revenue shown in Fig. 6(b).

From Fig. 6(b), it is observed that the NC scheme provides the lower-bound of total revenue of slices. In addition, the CVCT system with the LD strategy reduces the total provisioning cost of slices by nearly 70% compared to the NC scheme, which correspondingly improves the total revenue of slices around 17-fold. On the other hand, the cooperation between RRSs improves the total revenue of slices around 69.9% compared to the NoCoop scheme.

In these schemes when the storage capacities are low, the HBV and MPV strategies have lower performances than those of our proposed LD and HD strategies, since they do not consider the flexible delivery opportunities. For instance, when the cache size percentage is 10%, the LD strategy outperforms the performance of the CVCT system by nearly 24.3% and 40.8% compared to HBV and MPV, respectively.

2) *Impact of the processing capacity of RRSs:* Fig. 7 shows the impact of processing capacity limitation at LP-RRSs on the performance of CPSs in different schemes. Obviously, larger processing capacities provide more video transcoding opportunities, which alleviate the backhaul resource usage. It is noted that two transcoding types exist in the system as self-transcoding and cooperative transcoding. The self-transcoding in the parallel transmission and transcoding

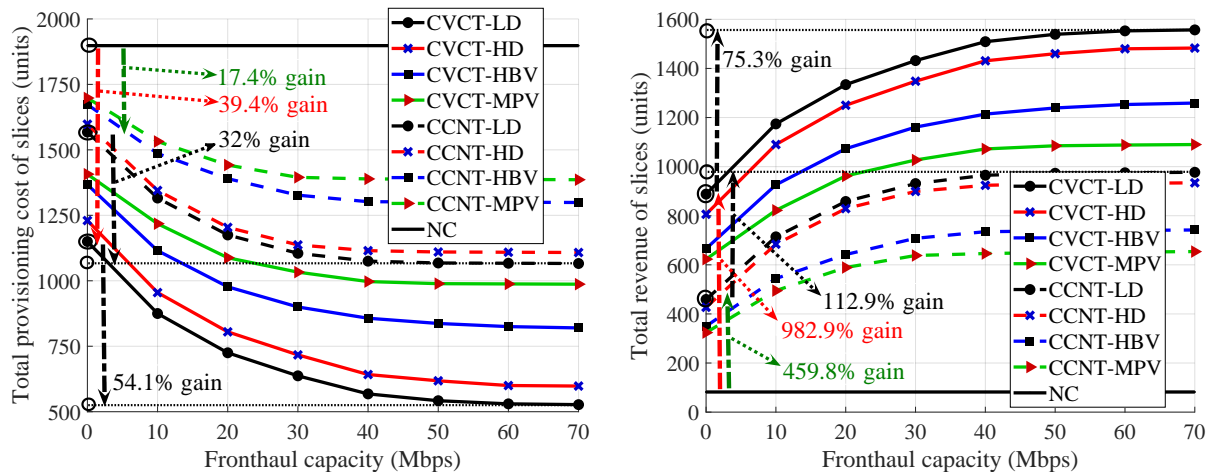
system mainly depends on the wireless channel, storage, and processing capacities. In other words, for larger processing capacities, increasing them alone cannot significantly improve the self-transcoding opportunities, since higher bitrate variants should be stored and the wireless channel capacities are limited. Besides, the cooperative transcoding mainly depends on the wireless channel, storage, processing and fronthaul link capacities. In other words, the cooperative transcoding operations cannot be successfully performed if the fronthaul capacities between RRSs are insufficient. Accordingly, based on the available storage and fronthaul capacities, it can be seen that the performance of all CPSs have slow changes when the processing capacity of LP-RRSs exceed 35 GHz and 15 GHz for the CVCT and NoCoop schemes, respectively. These results are shown in Fig. 7.

In Fig. 7(b), it is shown that the LD strategy in the CCNT scheme performs 10 times better than NC. Moreover, the cooperative transcoding technology improves the systems performance closed to 56.4% alone in the cooperative schemes when the processing capacity of LP-RRSs is 25 GHz.

As shown in Fig. 7, the performance of HBV is more affected by the amount of the processing capacity, since HBV randomly selects the highest bitrate variants in order to increase the self and (empirically) cooperative transcoding opportunities. Interestingly, when the relative processing capacities increase, the performance gain between the HBV and LD strategies decreases from 37.9% to 21.8%, as shown in Fig. 7(b). Therefore, the HBV strategy can be a good candidate when processing capacities are large enough. Besides, the performance of MPV changes slowly according to variations in processing capacity, since it does not consider the transcoding of video files, specifically in the event that low bitrate variants turn out to be more popular. MPV also stores the same popular videos, which significantly degrades the cooperative transcoding opportunity in the system.

3) *Impact of the fronthaul capacity of RRSs:* Fig. 8 shows the impact of the fronthaul capacity limitation between RRSs on the performance of CPSs in the CVCT and CCNT schemes. Generally, larger fronthaul capacities increase the cooperative communication capability. In this way, the systems performance will significantly be improved (see Fig. 8(b)).

According to Fig. 8(b), for the LD strategy, the CVCT technology with $R_{b',b}^{\max} = 70$ Mbps outperforms the total revenue of slices by nearly 75.3% compared to the NoCoop where $R_{b',b}^{\max} = 0$. In this regard, the systems performance is improved nearby 112.9% in the CCNT scheme which is caused only by the cooperative caching technology. Besides, the caching capability without



(a) Total provisioning cost of slices vs. fronthaul capacity between RRSs. (b) Total revenue of slices vs. fronthaul capacity between RRSs.

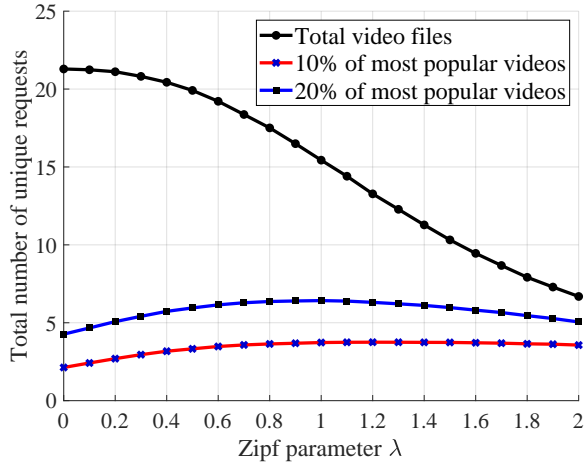
Fig. 8: Impact of fronthaul capacities between RRSs on performance of CPSs in different schemes.

any cooperation causes nearly 459.8% improvement in the total revenue of slices. In addition, the joint caching and transcoding capability at RRSs without any cooperation improves the system performance by nearly 10-fold compared to the NC scheme. From this result, it can be concluded that the self-transcoding capability in the system improves the total revenue of slices up to 5-fold alone.

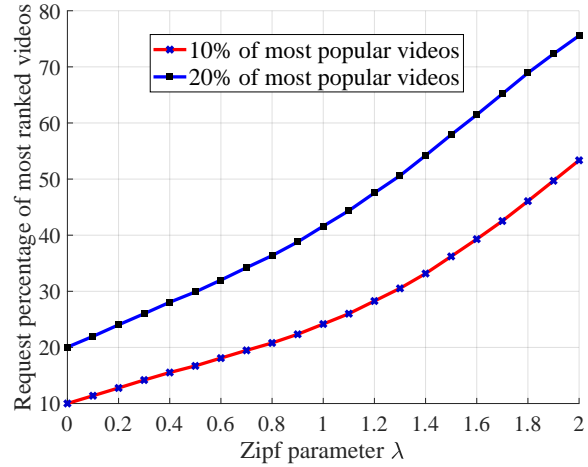
C. Effect of Zipf Parameter

Fig. 9 shows the effect of Zipf parameter λ on the performance of different CPSs. As shown in Fig. 9(a), for $\lambda = 1.5$, $U = 30$, and $VL = 40$, there are nearly 10 unique requests. For the aforementioned setting, Fig. 9(b) shows that nearly 57.9% and 36.22% of these requests are for 20% and 10% of most popular videos, respectively. These results are averaged over 10000 sets of requests. Accordingly, Figs. 9(a) and 9(b) show that when λ increases, the diversity of requests decreases in the system. In this line, the request percentage of the most ranked videos increases, exponentially in the system. In this regard, the backhaul, fronthaul, and processing resource usages are reduced which decrease the total provisioning cost of slices (shown in Fig. 9(c)). As a result, the total revenue of slices is improved that is shown in Fig. 9(d).

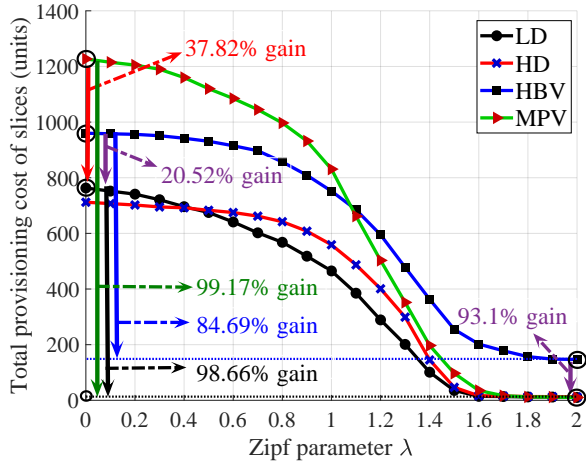
Based on Figs. 9(c) and 9(d), it can be derived that the HD strategy is more compatible than that of LD when λ tends to zero. Besides, MPV is more affected by the Zipf parameter, since it



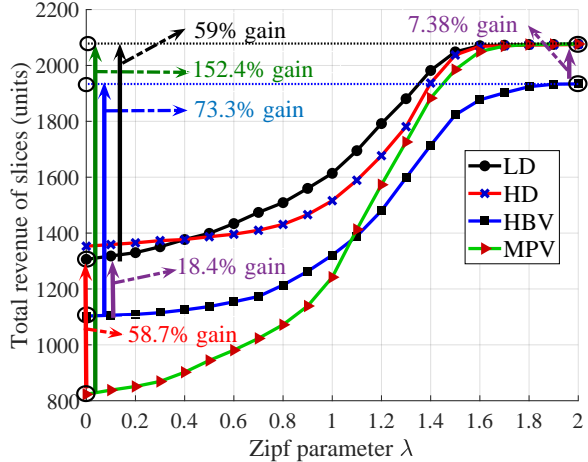
(a) Total number of unique requests vs. Zipf parameter for different video categorizes.



(b) Request percentage of most ranked videos vs. Zipf parameter for different video categorizes.



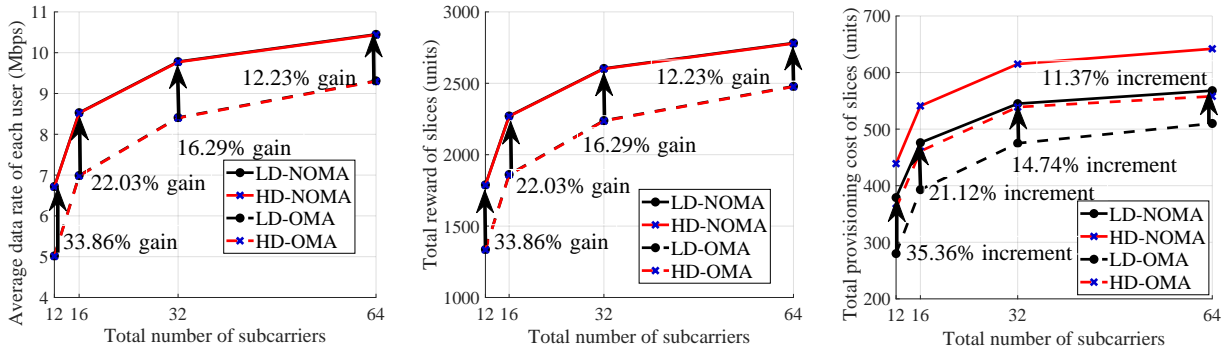
(c) Total provisioning cost of slices vs. Zipf parameter.



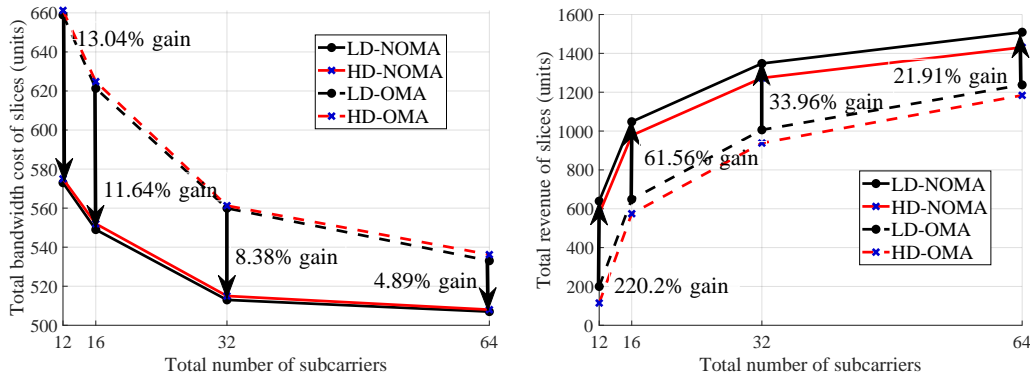
(d) Total revenue of slices vs. Zipf parameter.

Fig. 9: Effect of the Zipf parameter on performance of different CPSs.

is only a baseline popular strategy. Specifically, when λ varies from 0 to 2, MPV outperforms by about 152.4%. For $\lambda = 0$, i.e., when users uniformly request videos, HBV is more compatible than that of MPV. This is because, in this situation, the VPD factor is not dominant at all. In addition, the performance gaps in terms of the total revenue of slices between the LD and HBV strategies and the LD and MPV strategies are nearly 18.4% and 57.8%, respectively. Interestingly, these results show that MPV is not compatible for high diversity situations, whereas HBV can be a good solution with its very low complexity structure. On the other hand, when λ is large enough, i.e., when only a few videos are frequently requested by users, the performance gaps



(a) Average data rate of each user vs. total number of subcarriers. (b) Total reward of slices vs. total number of subcarriers. (c) Total provisioning cost of slices vs. total number of subcarriers.



(d) Total bandwidth cost of slices vs. total number of subcarriers. (e) Total revenue of slices vs. total number of subcarriers.

Fig. 10: Effect of the total number of subcarriers on performance of the LD and HD strategies in the MC-NOMA and OMA schemes.

between our proposed LD and HD strategies and MPV decrease significantly in the system. Actually, MPV is close to an almost optimal strategy when λ is too large. It is noted that there still exists a performance gap (nearly 7.38% in terms of total revenue of slices) between HBV and other strategies when λ is too large, since HBV does not consider the VPD.

D. Comparison Between MC-NOMA and OMA

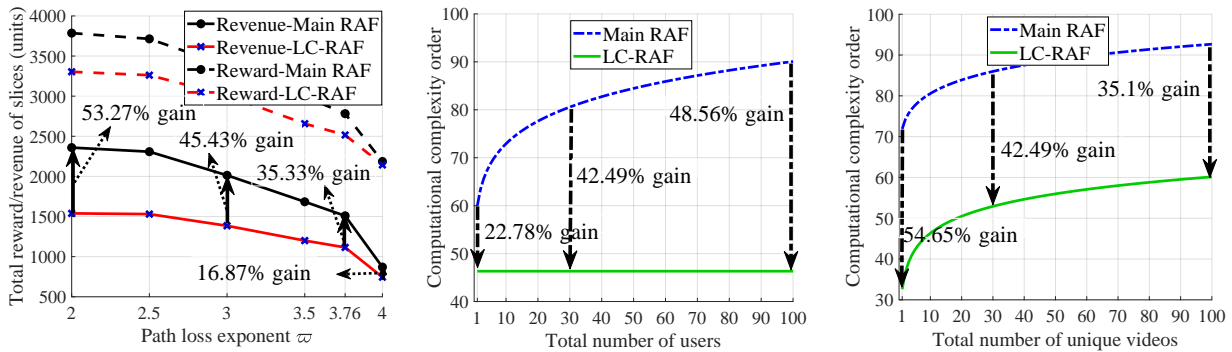
Fig. 10 compares the performance of MC-NOMA and OMA in the LD and HD strategies for different values of total number of subcarriers N . Generally, increasing N in multicarrier wireless networks improves the spectral efficiency of users. In this regard, the average data rate of users increases, as shown in Fig. 10(a). This improvement outperforms the total reward of slices (see

Fig. 10(b)). Paradoxically, increasing the data rate of users needs more backhaul, fronthaul, and processing resources due to the parallel delay constraints (12), (13), (15), (17), and (18). In this regard, improving the users access data rate leads to increasing the provisioning cost of slices which is shown in Fig. 10(c). Interestingly, by increasing N , the expensive wireless bandwidth usage is significantly reduced, which corresponds to a decrease in the total bandwidth cost. (see Fig. 10(d)). This is because increasing N improves the flexibility of bandwidth allocation in the multicarrier systems. Hence, more opportunities are provided for slices to assign the available subcarriers to the users and satisfy the QoS requirements. The bandwidth cost reduction and slice reward increments combined have a greater effect on the revenue of slices than the increment of the provisioning costs. Hence, increasing N improves the total revenue of slices as shown in Fig. 10(e).

MC-NOMA is expected to increase the spectral efficiency more than OMA by performing SIC at receivers shown in Fig. 10(a). In this regard, the total reward of slices is improved in the system (see Fig. 10(b)). Although MC-NOMA causes more provisioning costs than OMA because of increasing access data rates in parallel systems (see Fig. 10(c)), it reduces the total bandwidth cost of slices much more than OMA. This is because each slice can use the same subcarriers for its own users in each cell, while the price of each subcarrier bandwidth is paid once in the cell by that slice (see (20)). This opportunity is only instantiated by MC-NOMA, since it provides the reuse of orthogonal subcarriers at each RRS. As shown in Fig. 10(a), for $N = 12$, the average data rate of each user in MC-NOMA is improved by nearly 33.86% compared to OMA. This is because when OMA is applied to a system with critically low number of subcarriers, system performance is degraded owing to the flexibility of the bandwidth reuse at each RRS being completely eliminated. Finally, MC-NOMA outperforms OMA by nearly 220.2% when $N = 12$; and when $N = 64$, this result is reduced to 21.91%.

E. Comparison Between Our Proposed Resource Allocation Frameworks

Fig. 11 compares the performance of our proposed LC-RAF to that of Fig. 2 in terms of total revenue of slices and computational complexity order of the delivery algorithm. In Fig. 11(a) we assume that the path loss is modeled as $128.1 + 10\varpi \log_{10}(d_{b,u}) + z_{b,u}$ in dB where the path loss exponent ϖ varies from 2 to 4. Obviously, when ϖ increases, the data rate of users decreases in the system. Accordingly, the total reward of slices degrades, which reduces the total revenue of slices. Interestingly, as seen in Fig. 11(a), the performance gap between the main and



(a) Total reward/revenue of slices vs. path loss exponent ϖ . (b) Delivery computational complexity order vs. total number of users. In this simulation, we set $t^0 = 1$, $\varrho = 1$ and $\epsilon^0 = e$. Moreover, we consider 3 iterations for both Algorithm 1 and the SCA approach. (c) Delivery computational complexity order vs. total number of unique videos. In this simulation, we set $t^0 = 1$, $\varrho = 1$ and $\epsilon^0 = e$. Moreover, we consider 3 iterations for both Algorithm 1 and the SCA approach.

Fig. 11: Performance comparison of our proposed RAFs in terms of total revenue of slices and computational complexity of the delivery algorithm for the LD strategy.

low-complexity frameworks is reduced from 53.27% to 16.87% when ϖ varies from 2 to 4. This is because for larger values of ϖ , the flexibility of the user association process as well as the impact of the variations of small-scale fading decrease in the network. In this regard, users are more restricted; instead of choosing the RRS that has the requested video, each user is associated with the RRS that can provide the required data rate without consuming extra bandwidth and power resources. On the other hand, the CVCT system can significantly compensate for this restriction to prevent the extra backhaul resource usages. From Fig. 11(a), it can be observed that our proposed LC-RAF is a good choice for environments with larger values of ϖ .

As can be seen in Figs. 11(b) and 11(c), the computational complexity of the delivery algorithm in the LC-RAF is reduced by nearly 48.56% and 35.1%, when the total number of users U and unique videos V are large enough, respectively. Interestingly, as shown in Fig. 11(b), the complexity of the delivery algorithm in the LC-RAF does not depend on the number of users, which means this framework can be a good choice for dense environments.

V. SUMMARY AND CONCLUDING REMARKS

In this paper, we investigated the idea of developing a DACPS in a parallel CVCT system followed by a limited backhaul and fronthaul MC-NOMA-assisted HV-MEC. In this network,

we first proposed a RAF based on the network operational time. In Phase 1, we designed two diversity-based schemes where in each scheme, we maximized the estimated average revenue of slices subject to the minimum required access data rate of each user owned by each slice and some fundamental system constraints. In order to find an efficient solution for these large-scale and NP-hard problems, we proposed a solution algorithm based on the alternating optimization method. To reduce the computational complexity of the delivery algorithm, we proposed a LC-RAF where the radio resource allocation policy obtained in Phase 1 is adopted for all time slots of Phase 2. Numerical assessments showed that our proposed DACPSs improve the average system delivery cost between 25% and 40% compared to the conventional baseline bitrate/popular video CPSs. It is also observed that the integration of cooperative caching and cooperative transcoding capabilities can improve the system revenue up to 17-fold, which is notable considering each technology alone outperforms the system revenue only 6 to 10-fold. Finally, we showed that our proposed LC-RAF can be a good choice for dense environments with high levels of path loss where the distance of users to RRSs is more pivotal for the user association decision than the placement of videos in order to satisfy the QoS of users.

APPENDIX A

EQUIVALENT TRANSFORMATION OF (31)

The optimization problem (31) can be transformed into the following equivalent form as

$$\max_{\phi, \mathbf{p}, \mathbf{r}^{\text{BH}}, \mathbf{r}^{\text{FH}}} \bar{\$}_{\text{tot}}^{\text{LD}} \quad (34\text{a})$$

s.t. (7)-(10), (21d), (29b),

$$\mathbb{E}_{\mathbf{h}} \left\{ h_{b,u}^n \left(I_{b,u'}^{\text{Intra},n} + I_{b,u'}^{\text{Inter},n} + \sigma_{b,u'}^n \right) \right\} > \mathbb{E}_{\mathbf{h}} \left\{ h_{b,u}^n \left(\sum_{\substack{v \in \mathcal{U}, v \neq u' \\ h_{b,v}^n > h_{b,u}^n}} p_{b,v}^n h_{b,u}^n + I_{b,u}^{\text{Inter},n} + \sigma_{b,u}^n \right) \right\},$$

$$\forall b \in \mathcal{B}, u, u' \in \mathcal{U}, n \in \mathcal{N}, \tau_{b,u}^n, \tau_{b,u'}^n > 0, \mathbb{E}_{\mathbf{h}} \{ h_{b,u}^n \} > \mathbb{E}_{\mathbf{h}} \{ h_{b,u'}^n \}, \quad (34\text{b})$$

$$t_{b',b}^{v_h, v_l} \frac{r_{b',b}^{v_l}}{s_{v_l}} \leq t_{b',b}^{v_h, v_l} \frac{\phi_{b'}^{v_h, v_l}}{\eta^{v_h, v_l} N_{\text{Cycle}}^{v_h, v_l}}, \quad (34\text{c})$$

$$w_{b',b}^{v_h, v_l} \frac{\phi_b^{v_h, v_l}}{\eta^{v_h, v_l} N_{\text{Cycle}}^{v_h, v_l}} \leq w_{b',b}^{v_h, v_l} \frac{r_{b',b}^{v_h}}{s_{v_h}}, \quad (34\text{d})$$

$$y_b^{v_h, v_l} \frac{\bar{r}_{b,u}^{\text{Ac}}}{s_{v_l}} \leq \frac{\phi_b^{v_h, v_l}}{\eta^{v_h, v_l} N_{\text{Cycle}}^{v_h, v_l}} y_b^{v_h, v_l}, \quad (34\text{e})$$

$$z_{b',b}^{v_l} \bar{r}_{b,u}^{\text{Ac}} \leq r_{b',b}^{v_l} z_{b',b}^{v_l}, \quad (34\text{f})$$

$$t_{b',b}^{v_h,v_l} \bar{r}_{b,u}^{\text{Ac}} \leq t_{b',b}^{v_h,v_l} r_{b',b}^{v_l}, \quad (34g)$$

$$w_{b',b}^{v_h,v_l} \frac{\bar{r}_{b,u}^{\text{Ac}}}{s_{v_l}} \leq w_{b',b}^{v_h,v_l} \frac{\phi_b^{v_h,v_l}}{\eta^{v_h,v_l} N_{\text{Cycle}}^{v_h,v_l}}, \quad (34h)$$

$$o_b^{v_l} \bar{r}_{b,u}^{\text{Ac}} \leq o_b^{v_l} r_{0,b}^{v_l}, \quad (34i)$$

$$\phi_b^{v_h,v_l} \geq 0. \quad (34j)$$

In this line, to tackle the fractional constraints (14), (16), and (24), we transform them into equivalent forms as (34c)-(34i). Note that (34e)-(34i) hold even $\bar{r}_{b,u}^{\text{Ac}} = 0$, i.e., user u is not connected to RRS b . We also note that in this transformation, (34c) and (34d) are turned into linear forms (with relaxed $\phi_b^{v_h,v_l}$). Constraints (22), (29b), and (34e)-(34i) are in non-convex forms due to the fractional form of SINR function $\gamma_{b,u}^n$, non-concavity and non-convexity of $\bar{r}_{b,u}^{\text{Ac}}$, respectively. However, (22) can be transformed into an equivalent linear form with respect to \mathbf{p} as (34b) meaning that (22) should be held when $\tau_{b,u}^n \tau_{b,u'}^n \neq 0$.

APPENDIX B

THE PROPOSED SCA ALGORITHM FOR SOLVING (34)

To tackle the non-convexity of both (34a) and (29b) and all constraints in (34e)-(34i), the access data rate function $\bar{r}_{b,u}^{\text{Ac}}$ should be transformed into concave and convex forms, respectively. To approximate the access data rate function $\bar{r}_{b,u}^{\text{Ac}}$ in (34a) and (29b) to a concave format at each iteration κ_2 of the SCA algorithm, we first define

$$r_{b,u}^n = f_{b,u}^n - g_{b,u}^n, \quad (35)$$

where $f_{b,u}^n$ and $g_{b,u}^n$ are concave functions with respect to \mathbf{p} . Moreover, $f_{b,u}^n$ and $g_{b,u}^n$ are formulated, respectively, by

$$f_{b,u}^n = \tau_{b,u}^n W_s \log_2 \left(I_{b,u}^{\text{Intra},n} + I_{b,u}^{\text{Inter},n} + \sigma_{b,u}^n + p_{b,u}^n h_{b,u}^n \right), \quad (36)$$

$$g_{b,u}^n = \tau_{b,u}^n W_s \log_2 \left(I_{b,u}^{\text{Intra},n} + I_{b,u}^{\text{Inter},n} + \sigma_{b,u}^n \right). \quad (37)$$

Then, we approximate $g_{b,u}^n(\mathbf{p}_{\kappa_2})$ at each iteration κ_2 by its first order Taylor series approximation around \mathbf{p}_{κ_2-1} as follows [38], [39]:

$$g_{b,u}^n(\mathbf{p}_{\kappa_2}) \approx g_{b,u}^n(\mathbf{p}_{\kappa_2-1}) + \nabla g_{b,u}^n(\mathbf{p}_{\kappa_2-1})(\mathbf{p}_{\kappa_2} - \mathbf{p}_{\kappa_2-1}), \quad (38)$$

where $\nabla g_{b,u}^n(\mathbf{p}_{\kappa_2-1})$ is a vector of length UB and its entry is obtained by

$$\nabla g_{b,u}^n(\mathbf{p}) = \begin{cases} 0, & \forall i = b, u' \in \mathcal{U}/\{u\}, h_{b,u'}^n \leq h_{b,u}^n; \\ \frac{\tau_{b,u}^n W_s h_{b,u}^n}{(\ln 2)(I_{b,u}^{\text{Intra},n} + I_{b,u}^{\text{Inter},n} + \sigma_{b,u}^n)}, & \forall i = b, u' \in \mathcal{U}/\{u\}, h_{b,u'}^n > h_{b,u}^n; \\ \frac{\tau_{b,u}^n W_s h_{i,u}^n}{(\ln 2)(I_{b,u}^{\text{Intra},n} + I_{b,u}^{\text{Inter},n} + \sigma_{b,u}^n)}, & \forall i \neq b, u' \in \mathcal{U}/\{u\}. \end{cases} \quad (39)$$

Therefore, the concave approximated function of $\bar{r}_{b,u}^n$ at each iteration κ_2 is expressed by

$$\hat{r}_{b,u}^n(\mathbf{p}_{\kappa_2}) \approx \mathbb{E}_{\mathbf{h}} \left\{ f_{b,u}^n(\mathbf{p}_{\kappa_2}) - g_{b,u}^n(\mathbf{p}_{\kappa_2-1}) - \nabla g_{b,u}^n(\mathbf{p}_{\kappa_2-1})(\mathbf{p}_{\kappa_2} - \mathbf{p}_{\kappa_2-1}) \right\}. \quad (40)$$

Besides, in order to approximate $\bar{r}_{b,u}^{\text{Ac}}$ in (34e)-(34i) to a convex form at each iteration κ_2 of the SCA algorithm, we first define $\bar{r}_{b,u}^{\text{Ac}}$ as a D.C. function in (35). Then, we approximate $f_{b,u}^n(\mathbf{p}_{\kappa_2})$ at each iteration κ_2 by its first order Taylor series approximation around \mathbf{p}_{κ_2-1} as

$$f_{b,u}^n(\mathbf{p}_{\kappa_2}) \approx f_{b,u}^n(\mathbf{p}_{\kappa_2-1}) + \nabla f_{b,u}^n(\mathbf{p}_{\kappa_2-1})(\mathbf{p}_{\kappa_2} - \mathbf{p}_{\kappa_2-1}), \quad (41)$$

where $\nabla f_{b,u}^n(\mathbf{p}_{\kappa_2-1})$ is a vector of length UB and its entry is expressed by

$$\nabla f_{b,u}^n(\mathbf{p}) = \begin{cases} \frac{\tau_{b,u}^n W_s h_{b,u}^n}{(\ln 2)(I_{b,u}^{\text{Intra},n} + I_{b,u}^{\text{Inter},n} + \sigma_{b,u}^n + p_{b,u}^n h_{b,u}^n)}, & \forall i = b, u' = u; \\ 0, & \forall i = b, u' \in \mathcal{U}/\{u\}, h_{b,u'}^n \leq h_{b,u}^n; \\ \frac{\tau_{b,u}^n W_s h_{b,u}^n}{(\ln 2)(I_{b,u}^{\text{Intra},n} + I_{b,u}^{\text{Inter},n} + \sigma_{b,u}^n + p_{b,u}^n h_{b,u}^n)}, & \forall i = b, u' \in \mathcal{U}/\{u\}, h_{b,u'}^n > h_{b,u}^n; \\ \frac{\tau_{b,u}^n W_s h_{i,u}^n}{(\ln 2)(I_{b,u}^{\text{Intra},n} + I_{b,u}^{\text{Inter},n} + \sigma_{b,u}^n + p_{b,u}^n h_{b,u}^n)}, & \forall i \neq b, u' \in \mathcal{U}/\{u\}. \end{cases} \quad (42)$$

Hence, the convex approximated form of $\bar{r}_{b,u}^n$ at each iteration κ_2 is given by

$$\tilde{r}_{b,u}^n(\mathbf{p}_{\kappa_2}) \approx \mathbb{E}_{\mathbf{h}} \left\{ f_{b,u}^n(\mathbf{p}_{\kappa_2-1}) + \nabla f_{b,u}^n(\mathbf{p}_{\kappa_2-1})(\mathbf{p}_{\kappa_2} - \mathbf{p}_{\kappa_2-1}) - g_{b,u}^n(\mathbf{p}_{\kappa_2}) \right\}. \quad (43)$$

By substituting $\hat{r}_{b,u}^n$ in (34a) and (29b) and $\tilde{r}_{b,u}^n$ in (34e)-(34i), the optimization problem (34) is transformed into an approximated DCP form which can be easily solved by utilizing efficient convex programming solutions, such as the Lagrange dual method or the CVX software [10], [17], [40], [44], [45].

APPENDIX C

EQUIVALENT TRANSFORMATION OF (32)

The resulting IDCP form of (32) is formulated as

$$\min_{\boldsymbol{\Upsilon}, \boldsymbol{\rho}, \boldsymbol{\theta}, \boldsymbol{\tau}, \boldsymbol{\vartheta}, \boldsymbol{\nu}, \hat{\boldsymbol{\Upsilon}}, \check{\boldsymbol{\Upsilon}}} \sum_{m \in \mathcal{M}} \bar{\$}_m^{\text{slice, Epi, 2}} \quad (44a)$$

s.t. (1), (3), (4), (8)-(10), (21b)-(21d), (25), (29b), (29c), (34c), (34d),

$$\frac{\mathbb{E}_{\mathbf{h}} \left\{ \sum_{n=1}^N \check{y}_{b,u}^{v_h, v_l, n} W_s \log_2(1 + \gamma_{b,u}^n) \right\}}{s_{v_l}} \leq \frac{\phi_b^{v_h, v_l}}{\eta^{v_h, v_l} N_{\text{Cycle}}^{v_h, v_l}} y_b^{v_h, v_l}, \forall u \in \mathcal{U}_m, \quad (44b)$$

$$\mathbb{E}_{\mathbf{h}} \left\{ \sum_{n=1}^N \check{z}_{b',b,u}^{v_l, n} W_s \log_2(1 + \gamma_{b,u}^n) \right\} \leq r_{b',b}^{v_l} z_{b',b}^{v_l}, \forall u \in \mathcal{U}_m, \quad (44c)$$

$$\frac{\mathbb{E}_{\mathbf{h}} \left\{ \sum_{n=1}^N \check{t}_{b',b,u}^{v_h, v_l, n} W_s \log_2(1 + \gamma_{b,u}^n) \right\}}{s_{v_l}} \leq t_{b',b}^{v_h, v_l} r_{b',b}^{v_l}, \forall u \in \mathcal{U}_m, \quad (44d)$$

$$\frac{\mathbb{E}_{\mathbf{h}} \left\{ \sum_{n=1}^N \check{w}_{b',b,u}^{v_h, v_l, n} W_s \log_2(1 + \gamma_{b,u}^n) \right\}}{s_{v_l}} \leq w_{b',b}^{v_h, v_l} \frac{\phi_b^{v_h, v_l}}{\eta^{v_h, v_l} N_{\text{Cycle}}^{v_h, v_l}}, \forall u \in \mathcal{U}_m, \quad (44e)$$

$$\mathbb{E}_{\mathbf{h}} \left\{ \sum_{n=1}^N \check{o}_{b,u}^{v_l, n} W_s \log_2(1 + \gamma_{b,u}^n) \right\} \leq o_b^{v_l} r_{0,b}^{v_l}, \forall u \in \mathcal{U}_m, \quad (44f)$$

$$\mathbb{E}_{\mathbf{h}} \left\{ \tau_{b,u}^n \frac{p_{b,u}^n h_{b,u}^n}{\sum_{\substack{v \in \mathcal{U}, v \neq u' \\ h_{b,v}^n > h_{b,u'}^n}} p_{b,v}^n h_{b,u}^n + I_{b,u}^{\text{Inter},n} + \sigma_{b,u}^n} \right\} > \mathbb{E}_{\mathbf{h}} \{ \tau_{b,u'}^n \gamma_{b,u'}^n \}, \forall b \in \mathcal{B}, u, u' \in \mathcal{U}, n \in \mathcal{N},$$

$$p_{b,u}^n, p_{b,u'}^n > 0, \mathbb{E}_{\mathbf{h}} \{ h_{b,u}^n \} > \mathbb{E}_{\mathbf{h}} \{ h_{b,u'}^n \}, \quad (44g)$$

$$\vartheta_b \geq \theta_{b,u}, \forall b \in \mathcal{B}, u \in \mathcal{U}, \quad \vartheta_b \in \{0, 1\}, \quad (44h)$$

$$x_b^{v_l} + \sum_{\substack{v_h \in \mathcal{V} \\ h > l}} y_b^{v_h, v_l} + \sum_{\substack{b' \in \mathcal{B} \\ b' \neq b}} z_{b',b}^{v_l} + \sum_{\substack{b' \in \mathcal{B} \\ b' \neq b}} \sum_{\substack{v_h \in \mathcal{V} \\ h > l}} (t_{b',b}^{v_h, v_l} + w_{b',b}^{v_h, v_l}) + o_b^{v_l} = \vartheta_b, \forall b \in \mathcal{B}, v_l \in \mathcal{V}, \quad (44i)$$

$$\tilde{\vartheta}_{b,m} \geq \theta_{b,u}, \forall b \in \mathcal{B}, u \in \mathcal{U}_m, \quad \tilde{\vartheta}_{b,m} \in \{0, 1\}, \quad (44j)$$

$$\nu_{b,m}^n \geq \tau_{b,u}^n, \forall b \in \mathcal{B}, n \in \mathcal{N}, u \in \mathcal{U}_m, \quad \nu_{b,m}^n \in \{0, 1\}, \quad (44k)$$

$$\hat{x}_{b,m}^{v_l} \leq x_b^{v_l}, \quad \hat{x}_{b,m}^{v_l} \leq \tilde{\vartheta}_{b,m}, \quad \hat{x}_{b,m}^{v_l} \geq x_b^{v_l} + \tilde{\vartheta}_{b,m} - 1, \quad \hat{x}_{b,m}^{v_l} \in \{0, 1\}, \quad (44l)$$

$$\hat{y}_{b,m}^{v_h, v_l} \leq y_b^{v_h, v_l}, \quad \hat{y}_{b,m}^{v_h, v_l} \leq \tilde{\vartheta}_{b,m}, \quad \hat{y}_{b,m}^{v_h, v_l} \geq y_b^{v_h, v_l} + \tilde{\vartheta}_{b,m} - 1, \quad \hat{y}_{b,m}^{v_h, v_l} \in \{0, 1\}, \quad (44m)$$

$$\hat{z}_{b',b,m}^{v_l} \leq z_{b',b}^{v_l}, \quad \hat{z}_{b',b,m}^{v_l} \leq \tilde{\vartheta}_{b,m}, \quad \hat{z}_{b',b,m}^{v_l} \geq z_{b',b}^{v_l} + \tilde{\vartheta}_{b,m} - 1, \quad \hat{z}_{b',b,m}^{v_l} \in \{0, 1\}, \quad (44n)$$

$$\hat{t}_{b',b,m}^{v_h, v_l} \leq t_{b',b}^{v_h, v_l}, \quad \hat{t}_{b',b,m}^{v_h, v_l} \leq \tilde{\vartheta}_{b,m}, \quad \hat{t}_{b',b,m}^{v_h, v_l} \geq t_{b',b}^{v_h, v_l} + \tilde{\vartheta}_{b,m} - 1, \quad \hat{t}_{b',b,m}^{v_h, v_l} \in \{0, 1\}, \quad (44o)$$

$$\hat{w}_{b',b,m}^{v_h, v_l} \leq w_{b',b}^{v_h, v_l}, \quad \hat{w}_{b',b,m}^{v_h, v_l} \leq \tilde{\vartheta}_{b,m}, \quad \hat{w}_{b',b,m}^{v_h, v_l} \geq w_{b',b}^{v_h, v_l} + \tilde{\vartheta}_{b,m} - 1, \quad \hat{w}_{b',b,m}^{v_h, v_l} \in \{0, 1\}, \quad (44p)$$

$$\hat{o}_{b,m}^{v_l} \leq o_b^{v_l}, \quad \hat{o}_{b,m}^{v_l} \leq \tilde{\vartheta}_{b,m}, \quad \hat{o}_{b,m}^{v_l} \geq o_b^{v_l} + \tilde{\vartheta}_{b,m} - 1, \quad \hat{o}_{b,m}^{v_l} \in \{0, 1\}, \quad (44q)$$

$$\check{y}_{b,u}^{v_h, v_l, n} \leq y_b^{v_h, v_l}, \quad \check{y}_{b,u}^{v_h, v_l, n} \leq \tau_{b,u}^n, \quad \check{y}_{b,u}^{v_h, v_l, n} \geq y_b^{v_h, v_l} + \tau_{b,u}^n - 1, \quad \check{y}_{b,u}^{v_h, v_l, n} \in \{0, 1\}, \quad (44r)$$

$$\check{z}_{b',b,u}^{v_l, n} \leq z_{b',b}^{v_l}, \quad \check{z}_{b',b,u}^{v_l, n} \leq \tau_{b,u}^n, \quad \check{z}_{b',b,u}^{v_l, n} \geq z_{b',b}^{v_l} + \tau_{b,u}^n - 1, \quad \check{z}_{b',b,u}^{v_l, n} \in \{0, 1\}, \quad (44s)$$

$$\check{t}_{b',b,u}^{v_h,v_l,n} \leq t_{b',b}^{v_h,v_l}, \quad \check{t}_{b',b,u}^{v_h,v_l,n} \leq \tau_{b,u}^n, \quad \check{t}_{b',b,u}^{v_h,v_l,n} \geq t_{b',b}^{v_h,v_l} + \tau_{b,u}^n - 1, \quad \check{t}_{b',b,u}^{v_h,v_l,n} \in \{0, 1\}, \quad (44t)$$

$$\check{w}_{b',b,u}^{v_h,v_l,n} \leq w_{b',b}^{v_h,v_l}, \quad \check{w}_{b',b,u}^{v_h,v_l,n} \leq \tau_{b,u}^n, \quad \check{w}_{b',b,u}^{v_h,v_l,n} \geq w_{b',b}^{v_h,v_l} + \tau_{b,u}^n - 1, \quad \check{w}_{b',b,u}^{v_h,v_l,n} \in \{0, 1\}, \quad (44u)$$

$$\check{o}_{b,u}^{v_l,n} \leq o_b^{v_l}, \quad \check{o}_{b,u}^{v_l,n} \leq \tau_{b,u}^n, \quad \check{o}_{b,u}^{v_l,n} \geq o_b^{v_l} + \tau_{b,u}^n - 1, \quad \check{o}_{b,u}^{v_l,n} \in \{0, 1\}, \quad (44v)$$

where $\bar{\mathcal{S}}_m^{\text{slice,Epi,2}} = \sum_{u \in \mathcal{U}_m} \sum_{b \in \mathcal{B}} \bar{r}_{b,u}^{\text{Ac}} \psi_m - \sum_{u \in \mathcal{U}_m} \sum_{b \in \mathcal{B}} \sum_{n \in \mathcal{N}} (p_{b,u}^n \alpha_b^{\text{Pow}}) - \sum_{b \in \mathcal{B}} \sum_{n \in \mathcal{N}} (\nu_{b,m}^n W_s \alpha_b^{\text{Sub}}) - \sum_{b \in \mathcal{B}} \sum_{v_l \in \mathcal{V}} \Delta_{v_l} \left(\hat{x}_{b,m}^{v_l} (s_{v_l} \mu_b^{\text{Cache}}) + \sum_{\substack{v_h \in \mathcal{V} \\ h > l}} \hat{y}_{b,m}^{v_h,v_l} (s_{v_h} \mu_b^{\text{Cache}} + \phi_b^{v_h,v_l} \mu_b^{\text{Proc}}) + \sum_{\substack{b' \in \mathcal{B} \\ b' \neq b}} \hat{z}_{b',b,m}^{v_l} (s_{v_l} \mu_{b'}^{\text{Cache}} + r_{b',b}^{v_l} \alpha^{\text{FH}}) + \sum_{\substack{b' \in \mathcal{B} \\ b' \neq b}} \sum_{\substack{v_h \in \mathcal{V} \\ h > l}} \hat{t}_{b',b,m}^{v_h,v_l} (s_{v_h} \mu_{b'}^{\text{Cache}} + \phi_{b'}^{v_h,v_l} \mu_{b'}^{\text{Proc}} + r_{b',b}^{v_l} \alpha^{\text{FH}}) + \sum_{\substack{b' \in \mathcal{B} \\ b' \neq b}} \sum_{\substack{v_h \in \mathcal{V} \\ h > l}} \hat{w}_{b',b,m}^{v_h,v_l} (s_{v_h} \mu_{b'}^{\text{Cache}} + r_{b',b}^{v_h} \alpha^{\text{FH}} + \phi_b^{v_h,v_l} \mu_b^{\text{Proc}}) + \hat{o}_{b,m}^{v_l} (r_{0,b}^{v_l} \alpha^{\text{BH}}) \right), \quad \boldsymbol{\vartheta} = [\vartheta_b], \quad \tilde{\boldsymbol{\vartheta}} = [\tilde{\vartheta}_{b,m}], \quad \boldsymbol{\nu} = [\nu_{b,m}^n], \quad \hat{\boldsymbol{\Upsilon}} = [\hat{x}, \hat{y}, \hat{z}, \hat{t}, \hat{w}, \hat{o}], \quad \hat{\boldsymbol{x}} = [\hat{x}_{b,m}^{v_l}], \quad \hat{\boldsymbol{y}} = [\hat{y}_{b,m}^{v_h,v_l}], \quad \hat{\boldsymbol{z}} = [\hat{z}_{b',b,m}^{v_l}], \quad \hat{\boldsymbol{t}} = [\hat{t}_{b',b,m}^{v_h,v_l}], \quad \hat{\boldsymbol{w}} = [\hat{w}_{b',b,m}^{v_h,v_l}], \quad \hat{\boldsymbol{o}} = [\hat{o}_{b,m}^{v_l}], \quad \check{\boldsymbol{\Upsilon}} = [\check{y}, \check{z}, \check{t}, \check{w}, \check{o}], \quad \check{\boldsymbol{y}} = [\check{y}_{b,u}^{v_h,v_l,n}], \quad \check{\boldsymbol{z}} = [\check{z}_{b',b,u}^{v_l,n}], \quad \check{\boldsymbol{t}} = [\check{t}_{b',b,u}^{v_h,v_l,n}], \quad \check{\boldsymbol{w}} = [\check{w}_{b',b,u}^{v_h,v_l,n}], \quad \text{and } \check{\boldsymbol{o}} = [\check{o}_{b,u}^{v_l,n}].$ In order to overcome the nonlinearity challenges in (32), we first transform (6) into an equivalent integer linear form in (44g) which should be held when $p_{b,u}^n, p_{b,u'}^n > 0$ and $h_{b,u}^n > h_{b,u'}^n$. In addition, by introducing a new binary variable ϑ_b , where

$$\vartheta_b \geq \theta_{b,u}, \forall b \in \mathcal{B}, \quad \vartheta_b \in \{0, 1\}, \quad (45)$$

constraint (23) can be transformed into an equivalent form as (44i) which is in an integer linear form with respect to the new variable ϑ_b and all variables in $\boldsymbol{\Upsilon}$ [46]. In the same line, by defining new variables $\tilde{\vartheta}_{b,m}$ and $\nu_{b,m}^n$ such that (44j) and (44k) are held, respectively, the term $\bar{\mathcal{S}}_m^{\text{slice,UB}}$ in (32a) is transformed into the following equivalent form as

$$\bar{\mathcal{S}}_m^{\text{slice,Epi,1}} = \sum_{u \in \mathcal{U}_m} \sum_{b \in \mathcal{B}} \bar{r}_{b,u}^{\text{Ac}} \psi_m - \sum_{u \in \mathcal{U}_m} \sum_{b \in \mathcal{B}} \sum_{n \in \mathcal{N}} (p_{b,u}^n \alpha_b^{\text{Pow}}) - \sum_{b \in \mathcal{B}} \sum_{n \in \mathcal{N}} (\nu_{b,m}^n W_s \alpha_b^{\text{Sub}}) - \sum_{b \in \mathcal{B}} \tilde{\vartheta}_{b,m} \bar{\mathcal{S}}_b^{\text{Cost,RRS}}, \quad (46)$$

which is still in the integer nonlinear form, because of binary bilinear products generated by multiplications of $\tilde{\vartheta}_{b,m}$ in all scheduling variables in $\boldsymbol{\Upsilon}$ in the term $\tilde{\vartheta}_{b,m} \bar{\mathcal{S}}_b^{\text{Cost,RRS}}$. To address this challenge, we utilize the following lemma to linearize each binary bilinear product.

Lemma 1. Assume that $x \in \{0, 1\}$ and $y \in \{0, 1\}$ are binary variables. The binary variable $z \in \{0, 1\}$ can be substituted with the binary bilinear product xy if $z \leq x$, $z \leq y$, and $z \geq x + y - 1$.

Proof. For each two binary variables x and y , the following equality is always satisfied: $xy = \min\{x, y\}$. By utilizing the epigraph technique and introducing a new binary variable $z \in \{0, 1\}$ such that $z \leq x$, $z \leq y$, and $z \geq x + y - 1$, the integer linear term z can be replaced with the integer nonlinear term xy . \square

Based on **Lemma 1**, by adding constraints (44l)-(44q), the binary variables $\hat{y}_{b,m}^{v_h, v_l}$, $\hat{z}_{b',b,m}^{v_l}$, $\hat{t}_{b',b,m}^{v_h, v_l}$, $\hat{w}_{b',b,m}^{v_h, v_l}$, and $\hat{o}_{b,m}^{v_l}$ are replaced with the binary bilinear products $y_b^{v_h, v_l} \tilde{\vartheta}_{b,m}$, $z_{b',b}^{v_l} \tilde{\vartheta}_{b,m}$, $t_{b',b}^{v_h, v_l} \tilde{\vartheta}_{b,m}$, $w_{b',b}^{v_h, v_l} \tilde{\vartheta}_{b,m}$, and $o_b^{v_l} \tilde{\vartheta}_{b,m}$ in (46), respectively, which turn (46) into a linear integer form.

To cope with the nonlinearity of delay functions in (14) and (16), and average access delay functions in (24), we utilize the transformation method presented in Appendix A. To this end, we first transform (14) and (16) into (34c) and (34d), respectively, where both of them are in integer linear forms. Besides, we transform constraints in (24) into (34e)-(34i) which are still in integer nonlinear forms with respect to Υ and θ . According to **Lemma 1**, by adding constraints (44r)-(44v), the binary variables $\check{y}_{b,u}^{v_h, v_l, n}$, $\check{z}_{b',b,u}^{v_l, n}$, $\check{t}_{b',b,u}^{v_h, v_l, n}$, $\check{w}_{b',b,u}^{v_h, v_l, n}$, and $\check{o}_{b,u}^{v_l, n}$ are replaced with the binary bilinear products $y_b^{v_h, v_l} \tau_{b,u}^n$, $z_{b',b}^{v_l} \tau_{b,u}^n$, $t_{b',b}^{v_h, v_l} \tau_{b,u}^n$, $w_{b',b}^{v_h, v_l} \tau_{b,u}^n$, and $o_b^{v_l} \tau_{b,u}^n$ in (34e)-(34i), respectively where the result constraints (44b)-(44f) are in integer linear forms.

APPENDIX D

EQUIVALENT TRANSFORMATION OF (30)

The first step of Algorithm 1, i.e., finding joint \mathbf{p} , ϕ , \mathbf{r}^{FH} and \mathbf{r}^{BH} , is similar to the first step of solving (29) except that in the second step, i.e., finding joint Υ , ρ , τ and θ , $\theta_{b,u}$ is directly multiplied to all scheduling variables in Υ . Therefore, by using **Lemma 1**, (30) is transformed into an equivalent IDCP problem formulated as

$$\min_{\Upsilon, \rho, \theta, \tau, \nu, \check{\Upsilon}, \check{\Upsilon}} \sum_{m \in \mathcal{M}} \bar{\$}_m^{\text{slice, Epi, LB}} \quad (47a)$$

$$\text{s.t. } (1), (3), (4), (8)-(10), (21b)-(21d), (25), (29b), (29c), (34c), (34d), (44b)-(44i), (44k), (44r)-(44v),$$

$$\tilde{x}_{b,u}^{v_l} \leq x_b^{v_l}, \quad \tilde{x}_{b,u}^{v_l} \leq \theta_{b,u}, \quad \tilde{x}_{b,u}^{v_l} \geq x_b^{v_l} + \theta_{b,u} - 1, \quad \tilde{x}_{b,u}^{v_l} \in \{0, 1\}, \quad (47b)$$

$$\tilde{y}_{b,u}^{v_h, v_l} \leq y_b^{v_h, v_l}, \quad \tilde{y}_{b,u}^{v_h, v_l} \leq \theta_{b,u}, \quad \tilde{y}_{b,u}^{v_h, v_l} \geq y_b^{v_h, v_l} + \theta_{b,u} - 1, \quad \tilde{y}_{b,u}^{v_h, v_l} \in \{0, 1\}, \quad (47c)$$

$$\tilde{z}_{b',b,u}^{v_l} \leq z_{b',b}^{v_l}, \quad \tilde{z}_{b',b,u}^{v_l} \leq \theta_{b,u}, \quad \tilde{z}_{b',b,u}^{v_l} \geq z_{b',b}^{v_l} + \theta_{b,u} - 1, \quad \tilde{z}_{b',b,u}^{v_l} \in \{0, 1\}, \quad (47d)$$

$$\tilde{t}_{b',b,u}^{v_h, v_l} \leq t_{b',b}^{v_h, v_l}, \quad \tilde{t}_{b',b,u}^{v_h, v_l} \leq \theta_{b,u}, \quad \tilde{t}_{b',b,u}^{v_h, v_l} \geq t_{b',b}^{v_h, v_l} + \theta_{b,u} - 1, \quad \tilde{t}_{b',b,u}^{v_h, v_l} \in \{0, 1\}, \quad (47e)$$

$$\tilde{w}_{b',b,u}^{v_h, v_l} \leq w_{b',b}^{v_h, v_l}, \quad \tilde{w}_{b',b,u}^{v_h, v_l} \leq \theta_{b,u}, \quad \tilde{w}_{b',b,u}^{v_h, v_l} \geq w_{b',b}^{v_h, v_l} + \theta_{b,u} - 1, \quad \tilde{w}_{b',b,u}^{v_h, v_l} \in \{0, 1\}, \quad (47f)$$

$$\tilde{o}_{b,u}^{v_l} \leq o_b^{v_l}, \quad \tilde{o}_{b,u}^{v_l} \leq \theta_{b,u}, \quad \tilde{o}_{b,u}^{v_l} \geq o_b^{v_l} + \theta_{b,u} - 1, \quad \tilde{o}_{b,u}^{v_l} \in \{0, 1\}, \quad (47g)$$

where $\tilde{\Upsilon} = [\tilde{\mathbf{x}}, \tilde{\mathbf{y}}, \tilde{\mathbf{z}}, \tilde{\mathbf{t}}, \tilde{\mathbf{w}}, \tilde{\mathbf{o}}]$, $\tilde{\mathbf{x}} = [\tilde{x}_{b,u}^{v_l}]$, $\tilde{\mathbf{y}} = [\tilde{y}_{b,u}^{v_h, v_l}]$, $\tilde{\mathbf{z}} = [\tilde{z}_{b',b,u}^{v_l}]$, $\tilde{\mathbf{t}} = [\tilde{t}_{b',b,u}^{v_h, v_l}]$, $\tilde{\mathbf{w}} = [\tilde{w}_{b',b,u}^{v_h, v_l}]$, $\tilde{\mathbf{o}} = [\tilde{o}_{b,u}^{v_l}]$ and $\bar{\mathcal{S}}_m^{\text{slice, Epi, LB}} = \sum_{u \in \mathcal{U}_m} \sum_{b \in \mathcal{B}} \bar{r}_{b,u}^{\text{Ac}} \psi_m - \sum_{u \in \mathcal{U}_m} \sum_{b \in \mathcal{B}} \sum_{n \in \mathcal{N}} (p_{b,u}^n \alpha_b^{\text{Pow}}) - \sum_{b \in \mathcal{B}} \sum_{n \in \mathcal{N}} (\nu_{b,m}^n W_s \alpha_b^{\text{Sub}}) -$

$$\sum_{b \in \mathcal{B}} \sum_{u \in \mathcal{U}_m} \sum_{v_l \in \mathcal{V}} \Delta_{v_l} \left(\tilde{x}_{b,u}^{v_l} (s_{v_l} \mu_b^{\text{Cache}}) + \sum_{\substack{v_h \in \mathcal{V} \\ h > l}} \tilde{y}_{b,u}^{v_h, v_l} (s_{v_h} \mu_b^{\text{Cache}} + \phi_b^{v_h, v_l} \mu_b^{\text{Proc}}) + \right.$$

$$\left. \sum_{\substack{b' \in \mathcal{B} \\ b' \neq b}} \tilde{z}_{b',b,u}^{v_l} (s_{v_l} \mu_{b'}^{\text{Cache}} + r_{b',b}^{v_l} \alpha^{\text{FH}}) + \sum_{\substack{b' \in \mathcal{B} \\ b' \neq b}} \sum_{\substack{v_h \in \mathcal{V} \\ h > l}} \tilde{t}_{b',b,u}^{v_h, v_l} (s_{v_h} \mu_{b'}^{\text{Cache}} + \phi_{b'}^{v_h, v_l} \mu_{b'}^{\text{Proc}} + r_{b',b}^{v_l} \alpha^{\text{FH}}) + \right.$$

$$\left. \sum_{\substack{b' \in \mathcal{B} \\ b' \neq b}} \sum_{\substack{v_h \in \mathcal{V} \\ h > l}} \tilde{w}_{b',b,u}^{v_h, v_l} (s_{v_h} \mu_{b'}^{\text{Cache}} + r_{b',b}^{v_h} \alpha^{\text{FH}} + \phi_b^{v_h, v_l} \mu_b^{\text{Proc}}) + \tilde{o}_{b,u}^{v_l} (r_{0,b}^{v_l} \alpha^{\text{BH}}) \right).$$

APPENDIX E

PROOF OF PROPOSITION 2

Each iteration κ_1 in the proposed Algorithm 1 for solving (29) consists of two main steps. In the first step, we find $(\mathbf{p}_{\kappa_1}, \phi_{\kappa_1}, \mathbf{r}_{\kappa_1}^{\text{FH}}, \mathbf{r}_{\kappa_1}^{\text{BH}})$ by solving (29) for a fixed $(\Upsilon_{\kappa_1-1}, \rho_{\kappa_1-1}, \tau_{\kappa_1-1}, \theta_{\kappa_1-1})$ using an equivalent transformation method and subsequently applying the iterative SCA Algorithm 2 which provides a local optimum solution for (29) that is proved in **Proposition 3**. In this line, we have the following relation

$$\bar{\mathcal{S}}_{\text{tot}}(\mathbf{p}_{\kappa_1-1}, \phi_{\kappa_1-1}, \mathbf{r}_{\kappa_1-1}^{\text{FH}}, \mathbf{r}_{\kappa_1-1}^{\text{BH}}, \Upsilon_{\kappa_1-1}, \rho_{\kappa_1-1}, \tau_{\kappa_1-1}, \theta_{\kappa_1-1}) \leq \bar{\mathcal{S}}_{\text{tot}}(\mathbf{p}_{\kappa_1}, \phi_{\kappa_1}, \mathbf{r}_{\kappa_1}^{\text{FH}}, \mathbf{r}_{\kappa_1}^{\text{BH}}, \Upsilon_{\kappa_1-1}, \rho_{\kappa_1-1}, \tau_{\kappa_1-1}, \theta_{\kappa_1-1}). \quad (48)$$

In the second step of iteration κ_1 , we find $(\Upsilon_{\kappa_1}, \rho_{\kappa_1}, \tau_{\kappa_1}, \theta_{\kappa_1})$ by solving (29) for the given $(\mathbf{p}_{\kappa_1}, \phi_{\kappa_1}, \mathbf{r}_{\kappa_1}^{\text{FH}}, \mathbf{r}_{\kappa_1}^{\text{BH}})$ from the previous step. In doing so, the INLP problem (29) is transformed into a IDCP from in (44) which is efficiently solved by using CVX with the internal solver MOSEK. Using the fact that CVX with the MOSEK solver improves the objective function (44a) or the objective function of its equivalent problem (29) for the given $(\mathbf{p}_{\kappa_1}, \phi_{\kappa_1}, \mathbf{r}_{\kappa_1}^{\text{FH}}, \mathbf{r}_{\kappa_1}^{\text{BH}})$, the following relation holds

$$\bar{\mathcal{S}}_{\text{tot}}(\mathbf{p}_{\kappa_1}, \phi_{\kappa_1}, \mathbf{r}_{\kappa_1}^{\text{FH}}, \mathbf{r}_{\kappa_1}^{\text{BH}}, \Upsilon_{\kappa_1-1}, \rho_{\kappa_1-1}, \tau_{\kappa_1-1}, \theta_{\kappa_1-1}) \leq \bar{\mathcal{S}}_{\text{tot}}(\mathbf{p}_{\kappa_1}, \phi_{\kappa_1}, \mathbf{r}_{\kappa_1}^{\text{FH}}, \mathbf{r}_{\kappa_1}^{\text{BH}}, \Upsilon_{\kappa_1}, \rho_{\kappa_1}, \tau_{\kappa_1}, \theta_{\kappa_1}). \quad (49)$$

According to (48) and (49), it can be easily observed that after each iteration κ_1 of Algorithm 1, the objective function (29a) is either improved or remains constant. Essentially, when the

iterations in Algorithm 1 continue, it will converge to a locally optimal solution. Note that since the solution approach in the first step of Algorithm 1, i.e, finding $(\mathbf{p}_{\kappa_1}, \phi_{\kappa_1}, \mathbf{r}_{\kappa_1}^{\text{FH}}, \mathbf{r}_{\kappa_1}^{\text{BH}})$ basically follows the SCA approach which converges to a locally optimal solution, the globally optimal solution $(\mathbf{p}_{\kappa_1}, \phi_{\kappa_1}, \mathbf{r}_{\kappa_1}^{\text{FH}}, \mathbf{r}_{\kappa_1}^{\text{BH}})$ can not be guaranteed and the performance gap from this locally optimal solution and the global solution is also unknown. To this end, their corresponding solutions $(\Upsilon_{\kappa_1}, \rho_{\kappa_1}, \tau_{\kappa_1}, \theta_{\kappa_1})$ maybe different. Accordingly, alternate Algorithm 1 cannot guarantee the global optimality of the solution for (29) and what can be proved is only the local optimality of the solution. Nevertheless, in [38], [47] is noted that the SCA method often empirically converges to a globally optimal solution.

APPENDIX F

PROOF OF PROPOSITION 3

In order to prove **Proposition 3**, we first prove that the proposed SCA-based Algorithm 2 generates a sequence of improved feasible solutions in equivalent problem of (31) which is formulated in (34). As discussed, in each iteration κ_2 of the SCA approach, $g_{b,u}^n(\mathbf{p}_{\kappa_2})$ is approximated with its first order Taylor series in (11) and $f_{b,u}^n(\mathbf{p}_{\kappa_2})$ is approximated with its first order Taylor series in (34e)-(34i). Indeed, $\nabla g_{b,u}^n(\mathbf{p}_{\kappa_2-1})$ and $\nabla f_{b,u}^n(\mathbf{p}_{\kappa_2-1})$ are supergradient functions of $g_{b,u}^n(\mathbf{p}_{\kappa_2-1})$ and $f_{b,u}^n(\mathbf{p}_{\kappa_2-1})$ for iteration $\kappa_2 - 1$, respectively. Since $g_{b,u}^n(\mathbf{p}_{\kappa_2})$ and $f_{b,u}^n(\mathbf{p}_{\kappa_2})$ are concave, it must be hold

$$g_{b,u}^n(\mathbf{p}_{\kappa_2}) \leq g_{b,u}^n(\mathbf{p}_{\kappa_2-1}) + \nabla g_{b,u}^n(\mathbf{p}_{\kappa_2-1})(\mathbf{p}_{\kappa_2} - \mathbf{p}_{\kappa_2-1}), \quad (50)$$

$$f_{b,u}^n(\mathbf{p}_{\kappa_2}) \leq f_{b,u}^n(\mathbf{p}_{\kappa_2-1}) + \nabla f_{b,u}^n(\mathbf{p}_{\kappa_2-1})(\mathbf{p}_{\kappa_2} - \mathbf{p}_{\kappa_2-1}), \quad (51)$$

at each iteration κ_2 , respectively. Using (40) and (43), the ergodic access data rate function $\bar{r}_{b,u}^n(\mathbf{p}_{\kappa_2})$ in (35) is approximated to a concave form $\hat{\bar{r}}_{b,u}^n(\mathbf{p}_{\kappa_2})$ in (11) and also to a convex form $\tilde{\bar{r}}_{b,u}^n(\mathbf{p}_{\kappa_2})$ in (34e)-(34i) at each iteration κ_2 . According to (35) and (50) it can be easily shown that the following relations hold

$$\begin{aligned} \bar{r}_{b,u}^n(\mathbf{p}_{\kappa_2}) &= \mathbb{E}_{\mathbf{h}} \{ f_{b,u}^n(\mathbf{p}_{\kappa_2}) - g_{b,u}^n(\mathbf{p}_{\kappa_2}) \} \geq \\ &\hat{\bar{r}}_{b,u}^n(\mathbf{p}_{\kappa_2}) = \mathbb{E}_{\mathbf{h}} \{ f_{b,u}^n(\mathbf{p}_{\kappa_2}) - g_{b,u}^n(\mathbf{p}_{\kappa_2-1}) - \nabla g_{b,u}^n(\mathbf{p}_{\kappa_2-1})(\mathbf{p}_{\kappa_2} - \mathbf{p}_{\kappa_2-1}) \}. \end{aligned} \quad (52)$$

Moreover, based on (35) and (51), we have

$$\bar{r}_{b,u}^n(\mathbf{p}_{\kappa_2}) = \mathbb{E}_{\mathbf{h}} \{ f_{b,u}^n(\mathbf{p}_{\kappa_2}) - g_{b,u}^n(\mathbf{p}_{\kappa_2}) \} \leq$$

$$\tilde{r}_{b,u}^n(\mathbf{p}_{\kappa_2}) = \mathbb{E}_{\mathbf{h}} \left\{ f_{b,u}^n(\mathbf{p}_{\kappa_2-1}) + \nabla f_{b,u}^n(\mathbf{p}_{\kappa_2-1})(\mathbf{p}_{\kappa_2} - \mathbf{p}_{\kappa_2-1}) - g_{b,u}^n(\mathbf{p}_{\kappa_2}) \right\}. \quad (53)$$

Besides, after solving the convex approximated problem of (34) in each iteration κ_2 , the following inequalities hold

$$\sum_{b \in \mathcal{B}} \sum_{n=1}^N \tilde{r}_{b,u}^n(\mathbf{p}_{\kappa_2}) \geq R_m^{\min}, \forall m \in \mathcal{M}, u \in \mathcal{U}_m, \quad (54)$$

$$y_b^{v_h, v_l} \frac{\sum_{n=1}^N \tilde{r}_{b,u}^n(\mathbf{p}_{\kappa_2})}{s_{v_l}} \leq \frac{\phi_b^{v_h, v_l}}{\eta^{v_h, v_l} N_{\text{Cycle}}^{v_h, v_l}} y_b^{v_h, v_l}, \quad (55)$$

$$z_{b',b}^{v_l} \sum_{n=1}^N \tilde{r}_{b,u}^n(\mathbf{p}_{\kappa_2}) \leq r_{b',b}^{v_l} z_{b',b}^{v_l}, \quad (56)$$

$$t_{b',b}^{v_h, v_l} \sum_{n=1}^N \tilde{r}_{b,u}^n(\mathbf{p}_{\kappa_2}) \leq t_{b',b}^{v_h, v_l} r_{b',b}^{v_l}, \quad (57)$$

$$w_{b',b}^{v_h, v_l} \frac{\sum_{n=1}^N \tilde{r}_{b,u}^n(\mathbf{p}_{\kappa_2})}{s_{v_l}} \leq w_{b',b}^{v_h, v_l} \frac{\phi_b^{v_h, v_l}}{\eta^{v_h, v_l} N_{\text{Cycle}}^{v_h, v_l}}, \quad (58)$$

and

$$o_b^{v_l} \sum_{n=1}^N \tilde{r}_{b,u}^n(\mathbf{p}_{\kappa_2}) \leq o_b^{v_l} r_{0,b}^{v_l}. \quad (59)$$

From (52)-(59), it can be concluded that

$$\sum_{b \in \mathcal{B}} \bar{r}_{b,u}^n(\mathbf{p}_{\kappa_2}) \geq R_m^{\min}, \forall m \in \mathcal{M}, u \in \mathcal{U}_m, \quad (60)$$

$$y_b^{v_h, v_l} \frac{\bar{r}_{b,u}^n(\mathbf{p}_{\kappa_2})}{s_{v_l}} \leq \frac{\phi_b^{v_h, v_l}}{\eta^{v_h, v_l} N_{\text{Cycle}}^{v_h, v_l}} y_b^{v_h, v_l}, \quad (61)$$

$$z_{b',b}^{v_l} \bar{r}_{b,u}^n(\mathbf{p}_{\kappa_2}) \leq r_{b',b}^{v_l} z_{b',b}^{v_l}, \quad (62)$$

$$t_{b',b}^{v_h, v_l} \bar{r}_{b,u}^n(\mathbf{p}_{\kappa_2}) \leq t_{b',b}^{v_h, v_l} r_{b',b}^{v_l}, \quad (63)$$

$$w_{b',b}^{v_h, v_l} \frac{\bar{r}_{b,u}^n(\mathbf{p}_{\kappa_2})}{s_{v_l}} \leq w_{b',b}^{v_h, v_l} \frac{\phi_b^{v_h, v_l}}{\eta^{v_h, v_l} N_{\text{Cycle}}^{v_h, v_l}}, \quad (64)$$

and

$$o_b^{v_l} \bar{r}_{b,u}^n(\mathbf{p}_{\kappa_2}) \leq o_b^{v_l} r_{0,b}^{v_l}, \quad (65)$$

which means the optimal solution generated for the convex approximated problem of (34) at each iteration κ_2 is feasible with respect to the nonconvex problem (34). Moreover, based on (52), we have

$$\begin{aligned} & \sum_{m \in \mathcal{M}} \left(\sum_{u \in \mathcal{U}_m} \sum_{b \in \mathcal{B}} \bar{r}_{b,u}^{\text{Ac}}(\mathbf{p}_{\kappa_2}^*) \psi_m - \sum_{u \in \mathcal{U}_m} \sum_{b \in \mathcal{B}} \sum_{n \in \mathcal{N}} (p_{b,u}^{n,(\kappa_2)} \alpha_b^{\text{Pow}}) - \sum_{b \in \mathcal{B}} \sum_{n \in \mathcal{N}} \left(\max_{u \in \mathcal{U}_m} \{\tau_{b,u}^n\} W_s \alpha_b^{\text{Sub}} \right) \right) \\ & - \sum_{b \in \mathcal{B}} \min \left\{ \sum_{u \in \mathcal{U}_m} \theta_{b,u}, 1 \right\} \bar{\Phi}_b^{\text{Cost,RRS}} \geq \sum_{m \in \mathcal{M}} \left(\sum_{u \in \mathcal{U}_m} \sum_{b \in \mathcal{B}} \sum_{n \in \mathcal{N}} (\hat{r}_{b,u}^n(\mathbf{p}_{\kappa_2}^*)) \psi_m - \sum_{u \in \mathcal{U}_m} \sum_{b \in \mathcal{B}} \sum_{n \in \mathcal{N}} (p_{b,u}^n \alpha_b^{\text{Pow}}) \right. \\ & \quad \left. - \sum_{b \in \mathcal{B}} \sum_{n \in \mathcal{N}} \left(\max_{u \in \mathcal{U}_m} \{\tau_{b,u}^n\} W_s \alpha_b^{\text{Sub}} \right) - \sum_{b \in \mathcal{B}} \min \left\{ \sum_{u \in \mathcal{U}_m} \theta_{b,u}, 1 \right\} \bar{\Phi}_b^{\text{Cost,RRS}} \right). \quad (66) \end{aligned}$$

By using the fact that the DCP approximated problem of (34) can be efficiently solved at each iteration κ_2 , where the globally optimal solution is in the feasible region of (34), it can be derived that

$$\begin{aligned} & \sum_{m \in \mathcal{M}} \left(\sum_{u \in \mathcal{U}_m} \sum_{b \in \mathcal{B}} \sum_{n \in \mathcal{N}} (\hat{r}_{b,u}^n(\mathbf{p}_{\kappa_2}^*)) \psi_m - \sum_{u \in \mathcal{U}_m} \sum_{b \in \mathcal{B}} \sum_{n \in \mathcal{N}} (p_{b,u}^{n,(\kappa_2)*} \alpha_b^{\text{Pow}}) - \sum_{b \in \mathcal{B}} \sum_{n \in \mathcal{N}} \left(\max_{u \in \mathcal{U}_m} \{\tau_{b,u}^n\} W_s \alpha_b^{\text{Sub}} \right) \right) \\ & - \sum_{b \in \mathcal{B}} \min \left\{ \sum_{u \in \mathcal{U}_m} \theta_{b,u}, 1 \right\} \bar{\Phi}_b^{\text{Cost,RRS}} = \max_{\phi_{\kappa_2}, \mathbf{p}_{\kappa_2}, \mathbf{r}_{\kappa_2}^{\text{BH}}, \mathbf{r}_{\kappa_2}^{\text{FH}}} \sum_{m \in \mathcal{M}} \left(\sum_{u \in \mathcal{U}_m} \sum_{b \in \mathcal{B}} \sum_{n \in \mathcal{N}} (\hat{r}_{b,u}^n(\mathbf{p}_{\kappa_2})) \psi_m - \right. \\ & \sum_{u \in \mathcal{U}_m} \sum_{b \in \mathcal{B}} \sum_{n \in \mathcal{N}} (p_{b,u}^{n,(\kappa_2)} \alpha_b^{\text{Pow}}) - \sum_{b \in \mathcal{B}} \sum_{n \in \mathcal{N}} \left(\max_{u \in \mathcal{U}_m} \{\tau_{b,u}^n\} W_s \alpha_b^{\text{Sub}} \right) - \sum_{b \in \mathcal{B}} \min \left\{ \sum_{u \in \mathcal{U}_m} \theta_{b,u}, 1 \right\} \bar{\Phi}_b^{\text{Cost,RRS}} \geq \\ & \sum_{m \in \mathcal{M}} \left(\sum_{u \in \mathcal{U}_m} \sum_{b \in \mathcal{B}} \sum_{n \in \mathcal{N}} (\mathbb{E}_{\mathbf{h}} \{f_{b,u}^n(\mathbf{p}_{\kappa_2-1}) - g_{b,u}^n(\mathbf{p}_{\kappa_2-1}) - \nabla g_{b,u}^n(\mathbf{p}_{\kappa_2-1})(\mathbf{p}_{\kappa_2-1} - \mathbf{p}_{\kappa_2-1})\}) \psi_m - \right. \\ & \sum_{u \in \mathcal{U}_m} \sum_{b \in \mathcal{B}} \sum_{n \in \mathcal{N}} (p_{b,u}^{n,(\kappa_2-1)} \alpha_b^{\text{Pow}}) - \sum_{b \in \mathcal{B}} \sum_{n \in \mathcal{N}} \left(\max_{u \in \mathcal{U}_m} \{\tau_{b,u}^n\} W_s \alpha_b^{\text{Sub}} \right) - \sum_{b \in \mathcal{B}} \min \left\{ \sum_{u \in \mathcal{U}_m} \theta_{b,u}, 1 \right\} \bar{\Phi}_b^{\text{Cost,RRS}} \Big) = \\ & \sum_{m \in \mathcal{M}} \left(\sum_{u \in \mathcal{U}_m} \sum_{b \in \mathcal{B}} \sum_{n \in \mathcal{N}} (\mathbb{E}_{\mathbf{h}} \{f_{b,u}^n(\mathbf{p}_{\kappa_2-1}) - g_{b,u}^n(\mathbf{p}_{\kappa_2-1})\}) \psi_m - \sum_{u \in \mathcal{U}_m} \sum_{b \in \mathcal{B}} \sum_{n \in \mathcal{N}} (p_{b,u}^{n,(\kappa_2-1)} \alpha_b^{\text{Pow}}) - \right. \\ & \quad \left. \sum_{b \in \mathcal{B}} \sum_{n \in \mathcal{N}} \left(\max_{u \in \mathcal{U}_m} \{\tau_{b,u}^n\} W_s \alpha_b^{\text{Sub}} \right) - \sum_{b \in \mathcal{B}} \min \left\{ \sum_{u \in \mathcal{U}_m} \theta_{b,u}, 1 \right\} \bar{\Phi}_b^{\text{Cost,RRS}} \right) = \\ & \sum_{m \in \mathcal{M}} \left(\sum_{u \in \mathcal{U}_m} \sum_{b \in \mathcal{B}} \sum_{n \in \mathcal{N}} (\bar{r}_{b,u}^n(\mathbf{p}_{\kappa_2-1})) \psi_m - \sum_{u \in \mathcal{U}_m} \sum_{b \in \mathcal{B}} \sum_{n \in \mathcal{N}} (p_{b,u}^{n,(\kappa_2-1)} \alpha_b^{\text{Pow}}) - \sum_{b \in \mathcal{B}} \sum_{n \in \mathcal{N}} \left(\max_{u \in \mathcal{U}_m} \{\tau_{b,u}^n\} W_s \alpha_b^{\text{Sub}} \right) \right) \\ & \quad - \sum_{b \in \mathcal{B}} \min \left\{ \sum_{u \in \mathcal{U}_m} \theta_{b,u}, 1 \right\} \bar{\Phi}_b^{\text{Cost,RRS}}. \quad (67) \end{aligned}$$

According to (66) and (67), it is obvious that

$$\begin{aligned}
& \sum_{m \in \mathcal{M}} \left(\sum_{u \in \mathcal{U}_m} \sum_{b \in \mathcal{B}} \bar{r}_{b,u}^{\text{Ac}}(\mathbf{p}_{\kappa_2}^*) \psi_m - \sum_{u \in \mathcal{U}_m} \sum_{b \in \mathcal{B}} \sum_{n \in \mathcal{N}} \left(p_{b,u}^{n,(\kappa_2)} \alpha_b^{\text{Pow}} \right) - \sum_{b \in \mathcal{B}} \sum_{n \in \mathcal{N}} \left(\max_{u \in \mathcal{U}_m} \{ \tau_{b,u}^n \} W_s \alpha_b^{\text{Sub}} \right) \right. \\
& \quad \left. - \sum_{b \in \mathcal{B}} \min \left\{ \sum_{u \in \mathcal{U}_m} \theta_{b,u}, 1 \right\} \bar{\$}_b^{\text{Cost,RRS}} \right) \geq \sum_{m \in \mathcal{M}} \left(\sum_{u \in \mathcal{U}_m} \sum_{b \in \mathcal{B}} \sum_{n \in \mathcal{N}} \left(\bar{r}_{b,u}^n(\mathbf{p}_{\kappa_2-1}) \right) \psi_m - \right. \\
& \quad \left. \sum_{u \in \mathcal{U}_m} \sum_{b \in \mathcal{B}} \sum_{n \in \mathcal{N}} \left(p_{b,u}^{n,(\kappa_2-1)} \alpha_b^{\text{Pow}} \right) - \sum_{b \in \mathcal{B}} \sum_{n \in \mathcal{N}} \left(\max_{u \in \mathcal{U}_m} \{ \tau_{b,u}^n \} W_s \alpha_b^{\text{Sub}} \right) - \sum_{b \in \mathcal{B}} \min \left\{ \sum_{u \in \mathcal{U}_m} \theta_{b,u}, 1 \right\} \bar{\$}_b^{\text{Cost,RRS}} \right),
\end{aligned} \tag{68}$$

which means after each iteration κ_2 of the proposed SCA approach for solving (34), the objective function (34a) which is exactly the same as (31a) is improved (increased) or remains constant. Accordingly, the proposed algorithm for solving (31) will converge to a local optimum solution.

REFERENCES

- [1] W. Jiang, G. Feng, and S. Qin, "Optimal cooperative content caching and delivery policy for heterogeneous cellular networks," *IEEE Transactions on Mobile Computing*, vol. 16, no. 5, pp. 1382–1393, May 2017.
- [2] N. Golrezaei, K. Shanmugam, A. G. Dimakis, A. F. Molisch, and G. Caire, "Femtocaching: Wireless video content delivery through distributed caching helpers," in *Proc. IEEE INFOCOM*, Orlando, FL, USA, Mar. 2012, pp. 1107–1115.
- [3] S. Rezvani, N. Mokari, M. R. Javan, and E. Jorswieck, "Fairness and transmission-aware caching and delivery policies in OFDMA-based HetNets," *IEEE Transactions on Mobile Computing*, pp. 1–1, Jan. 2019.
- [4] H. Ahlehagh and S. Dey, "Video-aware scheduling and caching in the radio access network," *IEEE/ACM Transactions on Networking*, vol. 22, no. 5, pp. 1444–1462, Oct. 2014.
- [5] X. Xu, J. Liu, and X. Tao, "Mobile edge computing enhanced adaptive bitrate video delivery with joint cache and radio resource allocation," *IEEE Access*, vol. 5, pp. 16 406–16 415, Aug. 2017.
- [6] H. A. Pedersen and S. Dey, "Enhancing mobile video capacity and quality using rate adaptation, RAN caching and processing," *IEEE/ACM Transactions on Networking*, vol. 24, no. 2, pp. 996–1010, Apr. 2016.
- [7] T. X. Tran, P. Pandey, A. Hajisami, and D. Pompili, "Collaborative multi-bitrate video caching and processing in mobile-edge computing networks," in *Proc. 13th Annual Conference on Wireless On-demand Network Systems and Services (WONS)*, Jackson, WY, USA, Feb. 2017, pp. 165–172.
- [8] T. X. Tran, A. Hajisami, P. Pandey, and D. Pompili, "Collaborative mobile edge computing in 5G networks: New paradigms, scenarios, and challenges," *IEEE Communications Magazine*, vol. 55, no. 4, pp. 54–61, Apr. 2017.
- [9] L. Wei, J. Cai, C. H. Foh, and B. He, "QoS-aware resource allocation for video transcoding in clouds," *IEEE Transactions on Circuits and Systems for Video Technology*, vol. 27, no. 1, pp. 49–61, Jan. 2017.
- [10] C. You, K. Huang, H. Chae, and B. H. Kim, "Energy-efficient resource allocation for mobile-edge computation offloading," *IEEE Transactions on Wireless Communications*, vol. 16, no. 3, pp. 1397–1411, Mar. 2017.
- [11] Y. Mao, J. Zhang, and K. B. Letaief, "Dynamic computation offloading for mobile-edge computing with energy harvesting devices," *IEEE Journal on Selected Areas in Communications*, vol. 34, no. 12, pp. 3590–3605, Dec. 2016.
- [12] J. Ren, G. Yu, Y. Cai, and Y. He, "Latency optimization for resource allocation in mobile-edge computation offloading," *IEEE Transactions on Wireless Communications*, vol. 17, no. 8, pp. 5506–5519, Aug. 2018.
- [13] P. Paymard, S. Rezvani, and N. Mokari, "Joint task scheduling and uplink/downlink radio resource allocation in PD-NOMA based mobile edge computing networks," *Physical Communication*, vol. 32, pp. 160–171, Jan. 2019.

- [14] C. F. Kao and C. N. Lee, "Aggregate profit-based caching replacement algorithms for streaming media transcoding proxy systems," *IEEE Transactions on Multimedia*, vol. 9, no. 2, pp. 221–230, Feb. 2007.
- [15] Z. Ding, P. Fan, G. K. Karagiannidis, R. Schober, and H. V. Poor, "NOMA assisted wireless caching: Strategies and performance analysis," *IEEE Transactions on Communications*, vol. 66, no. 10, pp. 4854–4876, Oct. 2018.
- [16] Z. Zhao, M. Xu, Y. Li, and M. Peng, "A non-orthogonal multiple access-based multicast scheme in wireless content caching networks," *IEEE Journal on Selected Areas in Communications*, vol. 35, no. 12, pp. 2723–2735, Dec. 2017.
- [17] Y. Sun, D. W. K. Ng, Z. Ding, and R. Schober, "Optimal joint power and subcarrier allocation for full-duplex multicarrier non-orthogonal multiple access systems," *IEEE Transactions on Communications*, vol. 65, no. 3, pp. 1077–1091, Mar. 2017.
- [18] K. Wang, H. Li, F. R. Yu, and W. Wei, "Virtual resource allocation in software-defined information-centric cellular networks with device-to-device communications and imperfect CSI," *IEEE Transactions on Vehicular Technology*, vol. 65, no. 12, pp. 10011–10021, Dec. 2016.
- [19] K. Wang, F. R. Yu, and H. Li, "Information-centric virtualized cellular networks with device-to-device (D2D) communications," *IEEE Transactions on Vehicular Technology*, vol. 65, no. 11, pp. 9319–9329, Nov. 2016.
- [20] X. Zhang and Q. Zhu, "Information-centric network virtualization for QoS provisioning over software defined wireless networks," in *Proc. IEEE Military Communications Conference (MILCOM)*, Baltimore, Maryland, Nov. 2016, pp. 1028–1033.
- [21] Z. Chen, J. Lee, T. Q. S. Quek, and M. Kountouris, "Cooperative caching and transmission design in cluster-centric small cell networks," *IEEE Transactions on Wireless Communications*, vol. 16, no. 5, pp. 3401–3415, May 2017.
- [22] J. Liu, B. Bai, J. Zhang, and K. B. Letaief, "Cache placement in fog-RANs: From centralized to distributed algorithms," *IEEE Transactions on Wireless Communications*, vol. 16, no. 11, pp. 7039–7051, Nov. 2017.
- [23] R. G. Stephen and R. Zhang, "Green OFDMA resource allocation in cache-enabled CRAN," in *Proc. IEEE Online Conference on Green Communications (OnlineGreenComm)*, Piscataway, NJ, USA, Nov. 2016, pp. 70–75.
- [24] Z. Tan, X. Li, F. R. Yu, L. Chen, H. Ji, and V. C. M. Leung, "Joint access selection and resource allocation in cache-enabled HCNs with D2D communications," in *Proc. IEEE Wireless Communications and Networking Conference (WCNC)*, San Francisco, CA, USA, Mar. 2017, pp. 1–6.
- [25] X. Peng, J. C. Shen, J. Zhang, and K. B. Letaief, "Backhaul-aware caching placement for wireless networks," in *Proc. IEEE Global Communications Conference (GLOBECOM)*, San Diego, CA, USA, Dec. 2015, pp. 1–6.
- [26] W. C. Ao and K. Psounis, "Fast content delivery via distributed caching and small cell cooperation," *IEEE Transactions on Mobile Computing*, vol. PP, no. 99, pp. 1–1, 2017.
- [27] X. Li, X. Wang, S. Xiao, and V. C. M. Leung, "Delay performance analysis of cooperative cell caching in future mobile networks," in *Proc. IEEE International Conference on Communications (ICC)*, London, England, June 2015, pp. 5652–5657.
- [28] Z. Ding, P. Fan, G. K. Karagiannidis, R. Schober, and H. V. Poor, "On the application of NOMA to wireless caching," in *Proc. IEEE International Conference on Communications (ICC)*, May 2018, pp. 1–7.
- [29] J. Zhao, Y. Liu, T. Mahmoodi, K. K. Chai, Y. Chen, and Z. Han, "Resource allocation in cache-enabled CRAN with non-orthogonal multiple access," in *Proc. IEEE International Conference on Communications (ICC)*, May 2018, pp. 1–6.
- [30] C. Liang, F. R. Yu, H. Yao, and Z. Han, "Virtual resource allocation in information-centric wireless networks with virtualization," *IEEE Transactions on Vehicular Technology*, vol. 65, no. 12, pp. 9902–9914, Dec. 2016.
- [31] G. Gao, H. Hu, Y. Wen, and C. Westphal, "Resource provisioning and profit maximization for transcoding in clouds: A two-timescale approach," *IEEE Transactions on Multimedia*, vol. 19, no. 4, pp. 836–848, Apr. 2017.

- [32] S. H. Park, O. Simeone, and S. S. Shitz, "Joint optimization of cloud and edge processing for fog radio access networks," *IEEE Transactions on Wireless Communications*, vol. 15, no. 11, pp. 7621–7632, Nov. 2016.
- [33] F. Cheng, Y. Yu, Z. Zhao, N. Zhao, Y. Chen, and H. Lin, "Power allocation for cache-aided small-cell networks with limited backhaul," *IEEE Access*, vol. 5, pp. 1272–1283, Jan. 2017.
- [34] J. Li, Y. Chen, Z. Lin, W. Chen, B. Vucetic, and L. Hanzo, "Distributed caching for data dissemination in the downlink of heterogeneous networks," *IEEE Transactions on Communications*, vol. 63, no. 10, pp. 3553–3568, Oct. 2015.
- [35] Y. Sun, D. W. K. Ng, Z. Ding, and R. Schober, "Optimal joint power and subcarrier allocation for MC-NOMA systems," in *Proc. IEEE Global Communications Conference (GLOBECOM)*, Washington, DC, USA, Dec. 2016.
- [36] Y. Fu, L. Salan, C. W. Sung, C. S. Chen, and M. Coupechoux, "Double iterative waterfilling for sum rate maximization in multicarrier NOMA systems," in *Proc. IEEE International Conference on Communications (ICC)*, Paris, France, May 2017.
- [37] L. Lei, D. Yuan, C. K. Ho, and S. Sun, "Joint optimization of power and channel allocation with non-orthogonal multiple access for 5G cellular systems," in *Proc. IEEE Global Communications Conference (GLOBECOM)*, San Diego, CA, USA, Dec. 2015.
- [38] D. T. Ngo, S. Khakurel, and T. Le-Ngoc, "Joint subchannel assignment and power allocation for OFDMA femtocell networks," *IEEE Transactions on Wireless Communications*, vol. 13, no. 1, pp. 342–355, Jan. 2014.
- [39] N. Mokari, F. Alavi, S. Parsaeefard, and T. Le-Ngoc, "Limited-feedback resource allocation in heterogeneous cellular networks," *IEEE Transactions on Vehicular Technology*, vol. 65, no. 4, pp. 2509–2521, Apr. 2016.
- [40] M. Grant and S. Boyd, "CVX: Matlab software for disciplined convex programming, version 2.1," Mar. 2014 [Online] Available: <http://cvxr.com/cvx>.
- [41] <https://www.mosek.com/products/mosek>.
- [42] GreenTouch, *Mobile communications WG architecture doc2: Reference scenarios*, May 2013.
- [43] A. P. Miettinen and J. K. Nurminen, "Energy efficiency of mobile clients in cloud computing," in *Proc. USENIX Conference on Hot Topics in Cloud Computing (HotCloud)*, Boston, MA, Jun. 2010.
- [44] A. Ben-Tal and A. Nemirovski, *Lectures on modern convex optimization analysis, algorithms, and engineering applications*. vol. 2. Siam, 2001.
- [45] M. Tao, E. Chen, H. Zhou, and W. Yu, "Content-centric sparse multicast beamforming for cache-enabled cloud RAN," *IEEE Transactions on Wireless Communications*, vol. 15, no. 9, pp. 6118–6131, Sep. 2016.
- [46] S. Boyd and L. Vandenberghe, *Convex Optimization*. Cambridge University Press, 2009.
- [47] H. H. Kha, H. D. Tuan, and H. H. Nguyen, "Fast global optimal power allocation in wireless networks by local D.C. programming," *IEEE Transactions on Wireless Communications*, vol. 11, no. 2, pp. 510–515, Feb. 2012.